CLM-R252

CLM-R252

UKAEA

Report

ASSESSMENT AND DEVELOPMENT OF THE BANKOFF AND HAN COARSE MIXING MODEL

D. F. Fletcher

CULHAM LABORATORY
Abingdon, Oxfordshire
1985

C.18

Available from H. M. Stationery Office

Price £6.00

CLM-R252

ASSESSMENT AND DEVELOPMENT OF THE BANKOFF AND HAN COARSE MIXING MODEL

D F FLETCHER

UKAEA, Culham Laboratory, Abingdon, Oxon, OX14 3DB

SUMMARY

The one-dimensional steady-state models of coarse mixing produced by Bankoff and Han [1] have been implemented and examined critically. Both the separated flow and homogeneous flow versions of the model are shown to give results which are very sensitive to the assumed initial conditions and it is concluded that these models make questionable assumptions about heat transfer mechanisms. Further calculations have shown that the predicted melt dispersion rates are a consequence of the particularly large heat transfer rates calculated from the chosen parameters and correlations. The models have been further developed and new calculations making more realistic assumptions about the radiation and film boiling heat transfer models give reduced dispersion. The extended model has also been used to investigate the effect of changing the continuous phase from water to steam, and allowing for melt and coolant breakup.

July, 1985

ISBN: 0-85311-139-1

CONTENTS

LIST OF FIGURES

NOMENCLATURE

A	Surface area
C_D	Drag coefficient
c_p	Specific heat capacity at constant pressure
D	Diameter
F_{ij}	Drag force per unit volume of phase i on phase j
g	Acceleration due to gravity
h	Heat transfer coefficient or specific enthalpy
h_{fg}	Enthalpy of vaporisation
k	Thermal conductivity
$\dot{m}_v$	Rate of vaporisation per unit volume
n_p	Number of particles per unit volume $\left(=6\alpha_m/\pi D_p^3\right)$
P	Pressure
Q	Energy transferred to fluid per unit volume $\left(=n_p A_p h_{tot}(T_m - T_{sat})\right)$
T	Temperature
u	Velocity
x	Quality
z	Distance

Greek symbols

α	Volume fraction
ε	Emissivity
ρ	Density
σ	Stefan-Boltzmann constant or surface tension
η	Parameter determining the fraction of the evaporation reaction force acting on each phase
δ	Vapour film thickness
μ	Dynamic viscosity

Subscripts

B	Bubble
c	Coolant
d	Dispersed phase

f	Fluid
fb	Film boiling
l	Liquid
m	Melt
p	Particle
r	Radiative
sat	Saturation
tot	Total (=radiation + film boiling)
v	Vapour

Superscripts

0	Condition at melt front

1 INTRODUCTION

In the study of hypothetical core degrading accidents the possibility of failure of the reactor containment due to a steam explosion has received considerable attention [2,3], but estimates of the probability of this event are somewhat uncertain. This is due both to the relatively poor knowledge of the complex physics involved in this process, and the difficulty of extrapolating from experimental results involving, say, 20kg of melt to the reactor situation where many tonnes of material would need to be involved in a coherent interaction before the integrity of the reactor containment would be threatened. For a melt/water interaction with a pouring mode of contact it is conventional to consider a steam explosion as a progression through the following stages:

(i) The melt and coolant mix together, with material zones having a characteristic length-scale of about 10mm. Due to the very high melt temperatures (3500K) the melt is surrounded by a vapour blanket, so that heat transfer rates are relatively low. During this stage, which develops over a period of the order of a second, the system is relatively quiescent and there is little pressure generation;

(ii) There is some initiating event which causes the vapour blanket to collapse locally, causing fragmentation of the melt, high heat transfer rates and pressurisation in some region of the mixture;

(iii) For a coherent interaction this must be followed by a propagation stage, where this disturbance creates a shock wave which propagates through the mixture causing fragmentation and rapid heat transfer from the melt to the coolant throughout the mixture [4, 26];

(iv) This is followed by an expansion stage during which the high pressure coolant expands doing work on its surroundings. Damage may result from either the high pressures produced or from the impact of material flowing out of the interaction zone.

The above description is somewhat simplified but it does highlight the crucial importance of being able to predict the effect of scale on mixing. Various models of this process have been produced but none are widely accepted [2] and some conflict with experimental evidence. Henry and Fauske [5] have produced a mixing limitation on the basis of steam flow separation of the melt and coolant. Their model uses a steady-state one-dimensional critical heat flux correlation. Corradini [6,7] has also produced a mixing model which places limits on mixing due to fluidization of either the melt or coolant. In the dynamic version of this model [7], results from the FITS experiments [8] are used to form correlations for melt dispersion, penetration, and mixing fragmentation size. These correlations are then used to model mixture development. Bankoff and Han [1] have produced a one-dimensional steady state model, a one-dimensional unsteady model, and a two-dimensional unsteady model based on the conservation laws of mass, momentum and energy.

A detailed review of these mixing models [31] has concluded that the models produced by Bankoff and coworkers are the most soundly based. Therefore, in this paper, the one-dimensional steady-state model of Bankoff and Han is described and examined critically. The treatment of radiation and film boiling heat transfer has been modified. The effect of changing the continuous phase from water to steam, and the effect of allowing for melt and coolant breakup have been examined.

2 BANKOFF AND HAN'S ONE DIMENSIONAL STEADY STATE MODEL

The model was formulated to apply to the situation where catastrophic and total failure of the lower core plate in a Light Water Reactor dumps melt into the water in the entire cross-sectional area of the plenum. The assumed geometry is shown in figure 1. In this event it is argued that the following assumptions can be made:

(i) The flows are one-dimensional.

This assumption is valid for a very specific contact mode between the melt and the coolant. In anything less than total failure of the lower core

plate the flow would be two dimensional (or most probably three dimensional), so that sideways inflow of water could occur. It is thought that the exclusion of this process is one of the major drawbacks of the model. Bankoff and Han do not consider what part the failed core plate plays in the mixing and its presence is ignored.

(ii) The flows are steady-state.

It is argued by Bankoff and Han that a steady state occurs because the particle settling time is much less than the time taken for the water/steam to pass through the mixture.

(iii) The front of the particles entering the water is plane with a specified and constant cross-sectional average volume fraction of particles. This is a consequence of assuming a one dimensional quasi-steady model and cannot be changed. This assumption is supported by experimental results which show a constant velocity melt front penetrating into the coolant [8].

(iv) All the melt is in spheres of the same size prior to mixing and the particle size remains fixed during mixing. This assumption is conventional and could be modified to incorporate a distribution of sizes by the method described in reference 10. It is thought that this modification is not worthwhile as this restriction is insignificant compared to some of the others. There is no information given about the method of melt particle production. A severe limitation is that the high steam velocities which develop could cause further breakup of the melt [11]. A modification to allow for this is given in section 5.4.

(v) The melt surface temperature is assumed constant. The validity of this assumption will depend on how rapidly the melt is dispersed and what heat transfer mechanisms are operating and is examined in section 5.5.

(vi) The coolant is assumed to be at its saturation temperature. This simplifies the modelling, as condensation does not have to be considered

and all the energy transferred to the water produces steam. Thus this situation is likely to be the most dispersive.

(vii) There is no pressurisation of the system by the steam produced.

Two different versions of the model were developed by Bankoff and Han, based on two different two-phase flow models. In the first the steam and water are treated as a homogeneous mixture and a standard homogeneous flow model is used. In the second the two phases are treated separately, so that each phase has a different velocity and occupies a separate volume of the flow channel. The second model is used for most of the calculations in this paper, as it is thought that this model is more appropriate at low pressure conditions where the two phases have densities differing by a factor of about 1600.

3 MODEL FORMULATION

The model is derived by using conservation of mass and momentum applied to the three phases and then making use of the assumptions listed above. A coordinate system moving with the melt front is used. The origin is taken to be at the melt front and the positive z direction is taken to be vertically upwards, as illustrated in figure 1.

3.1 Conservation of mass

Applying the principle of conservation of mass to each coolant phase in turn gives the following equations;

$$\frac{d}{dz}(\alpha_v \rho_v u_v) = \dot{m}_v \qquad \text{(vapour)} \quad (1)$$

$$\frac{d}{dz}(\alpha_l \rho_l u_l) = -\dot{m}_v \qquad \text{(liquid)} \quad (2)$$

where $\dot{m}_v$ is the mass rate of vaporisation of liquid per unit volume and is given by

$$\dot{m}_v = 6\alpha_m h_{tot}(T_m - T_{sat})/D_p h_{fg} \qquad (3)$$

Conservation of mass applied to the melt gives:

$$\frac{d}{dz}(\alpha_m \rho_m u_m) = 0 \qquad \text{(melt)} \quad (4)$$

but since $u_m=0$ at $z=0$, equation (4) shows that $u_m=0$ for all z.

3.2 Conservation of momentum

Conservation of momentum applied to the vapour, liquid and melt gives the following equations:

$$\alpha_v \rho_v u_v \frac{du_v}{dz} = -\alpha_v \frac{dp}{dz} - \alpha_v \rho_v g - F_{lv} - F_{mv}$$

$$- \eta(u_v - u_l)\,\dot{m}_v \qquad \text{(vapour)} \quad (5)$$

$$\alpha_l \rho_l u_l \frac{du_l}{dz} = -\alpha_l \frac{dp}{dz} - \alpha_l \rho_l g + F_{lv} - F_{ml}$$

$$-(1 - \eta)(u_v - u_l)\dot{m}_v \qquad \text{(liquid)} \quad (6)$$

$$\alpha_m \rho_m u_m \frac{du_m}{dz} = 0 = -\alpha_m \frac{dp}{dz} - \alpha_m \rho_m g + F_{mv} + F_{ml} \qquad \text{(melt)} \quad (7)$$

Equation (7) can be used to eliminate the pressure gradient term from equations (5) and (6) to give:

$$\alpha_v \rho_v u_v \frac{du_v}{dz} = \alpha_v(\rho_m - \rho_v) - F_{lv} - F_{mv}$$

$$- \frac{\alpha_v}{\alpha_m}(F_{mv} + F_{ml}) - \eta(u_v - u_l)\,\dot{m}_v \qquad (8)$$

$$\alpha_l \rho_l u_l \frac{du_l}{dz} = \alpha_l(\rho_m - \rho_l)\, g + F_{lv} - F_{ml}$$

$$- \frac{\alpha_l}{\alpha_m} (F_{mv} + F_{ml}) - (1 - \eta)(u_v - u_l)\, \dot{m}_v \qquad (9)$$

Thus equations (1), (2), (8) and (9) give four simultaneous ordinary differential equations in u_v, u_l, α_v and α_l. To close the system models for the drag forces, heat transfer, and evaporation reaction force have to be specified.

3.3 Drag models

There are three drag terms that need to be modelled; the drag of the liquid on the vapour, the melt on the vapour, and the melt on the liquid. Now since $u_v > u_l > u_m$ all the above drag forces will be positive. Since the liquid is assumed to be the continuous phase the drag of the vapour on the melt is set to zero. The drag force on a single particle is assumed to take the form

$$f_{ij} = 1/2\ C_D \rho_j \pi \frac{D_i^2}{4} (u_j - u_i) \left| u_j - u_j \right| \qquad (10)$$

and the number of particles per unit volume is given by

$$n_p = 6\alpha_m / \pi D_p^3 \qquad (11)$$

so that

$$F_{ij} = 3/4\ C_D \rho_j D_i^2 (u_j - u_i) \left| u_j - u_i \right| \alpha_m / D_p^3 \qquad (12)$$

It now only remains to determine appropriate drag coefficients.

To evaluate the drag of the liquid on the particles, the melt particle surrounded by its vapour blanket was considered to be a bubble with the particle diameter. The appropriate drag coefficient was obtained from reference 12 and is given by

$$C_D = 0.45 \left[\frac{1 + 17.67(1 - \alpha_m)^{9/7}}{18.67(1 - \alpha_m)^{3/2}}\right]^2 \qquad (13)$$

To evaluate the drag of the liquid on the vapour, the vapour was assumed to be a bubble of the same radius as the particle. Assuming the flow regime to be churn-turbulent the appropriate drag coefficient can be obtained from reference 12 and takes the form

$$C_B = \frac{8}{3}\left(1 - \alpha_v/(\alpha_v + \alpha_l)\right)^2 \qquad (14)$$

To summarise, the three drag forces per unit volume are

$$F_{mv} = 0$$

$$F_{ml} = 3/4\ C_D \rho_l u_l \left|u_l\right| \alpha_m / D_p$$

$$F_{lv} = 3/4\ C_B \rho_l (u_v - u_l) \left|u_v - u_l\right| \alpha_m / D_p \qquad (15)$$

The above drag coefficients seem to be the correct choice when the mixture consists of particles surrounded by relatively thin vapour blankets. Their use seems less justifiable when the melt becomes dispersed and there are large volume fractions of steam.

3.4 Heat transfer models

The heat transfer model consists of two components, namely radiation and film boiling. The film boiling heat transfer coefficient used by Bankoff and Han was that obtained by Witte [13] for forced convection film boiling around a sphere and is given by

$$h_{fb} = 2.98 \left[\frac{\rho_v k_v (h_{fg} + 0.68\ C_{pv}(T_m - T_{sat})u_l}{D_p (T_m - T_{sat})}\right]^{1/2} \qquad (16)$$

The above correlation was obtained by making the following assumptions:

(i) Saturated coolant

(ii) Laminar flow of the vapour

(iii) Radiative heat transfer may be neglected

(iv) The vapour film becomes so thick at 90 degrees around from the stagnation point that there is no further contribution to heat transfer from conduction across the remainder of the film.

The above assumptions do not seem valid in the present situation, where the vapour production rate is very large, due to the high temperature difference between the melt and the coolant. In particular, assumptions (ii) and (iii) seem likely to be in error because the large radiation heat flux will modify the vapour film thickness considerably and the vapour flow will probably be turbulent. The sensitivity of the model predictions to the assumed film boiling model will be examined in section 5.2.

The radiation heat transfer model used by Bankoff and Han assumes both the melt and coolant to be gray bodies. Thus,

$$h_r = \sigma F(T_m^4 - T_{sat}^4)/(T_m - T_{sat}) \tag{17}$$

where F is the radiation view factor and is given by [14]

$$F = \left[\frac{1-\varepsilon_m}{\varepsilon_m} + \frac{1}{F_{ml}} + \left(\frac{A_m}{A_l}\right)\left(\frac{1-\varepsilon_l}{\varepsilon_l}\right)\right]^{-1} \tag{18}$$

where F_{ml} is the fraction of radiant energy leaving the surface of the melt incident on the surface of the coolant.

Bankoff and Han assume that all the radiation leaving the melt is incident on coolant, that the emissivity of the water is in the range 0.95-0.963, and that the melt emissivity is in the range 0.6-0.85.

On the basis of these assumptions expression (18) can be approximated by

$$F = \varepsilon_m \qquad (19)$$

The above assumptions are by no means unquestionable. Firstly, it may be correct to assume that all the radiation leaving the melt is incident on water when the particle is surrounded by a thin vapour blanket. However, once large vapour volume fractions occur this assumption is very questionable as the vapour will be relatively transparent to steam (at low pressures anyway) and so the particles will radiate to each other. Secondly, the emissivity of the water seems far too high. At temperatures of say 1000K it only takes a fraction of a millimetre of water to absorb virtually all the emitted radiation [15]. However, at melt temperatures of 3500K a large proportion of the energy spectrum falls in the visible range where absorption lengths are of the order of metres. In fact at 3500K the peak radiation intensity occurs at 1μm, where the absorption length is about 10mm [16,10]. These issues are examined in detail in Appendix 1. Calculations using improved heat transfer models are described in section 5.1.

Bankoff and Han obtained the total heat transfer coefficient by adding together the separate heat transfer coefficients for radiation and film boiling. This assumption may not be valid due to the influence of the radiation heat transfer on the film boiling model. However, since no heat transfer model which combined radiation and film boiling could be found it was decided to simply add the heat transfer coefficients in the present study.

3.5 Evaporation reaction force

The last term in each of equations (5) and (6) is due to the transfer of momentum caused by the coolant phase change. As the vapour is moving with a different velocity to the liquid the evaporation mass flux will cause a transfer of momentum, which can be thought of as an

evaporative reaction force [17]. It is not clear how much of this force should be attributed to each phase, so the parameter η is introduced to enable its effect to be studied. Bankoff and Han used a value of $\eta=0$, which was obtained by giving each phase an interfacial velocity, as well as a bulk velocity, and then setting the interfacial velocities equal to the bulk vapour velocity.

Different workers have used various values of η; reference 18 cites examples where $\eta=1$ has been used in flows with net evaporation but does not agree with this value as there is then no jump in the liquid tangential velocity at the interface between the vapour and liquid. An elaborate weighting scheme, involving interface friction factors was suggested to overcome this. Wallis [17] notes that if $\eta=0.5$ the flows can be reversible. In the present study calculations using values of η in the range 0 to 1 have been made. It was found that the results were insensitive to the value of η and a value of $\eta=1$ was used in all subsequent calculations. In this case the evaporation force acts only on the vapour. It is not clear from the available literature which is the correct value to use. A value of $\eta=1$ was chosen because this was the value used by most workers modelling a flow with evaporation.

3.6 Initial conditions

The required initial conditions are velocities for the vapour and liquid, and volume fractions for any two of the three phases. One condition used by Bankoff and Han was to specify the initial volume fraction of particles at the melt front, which is particularly appropriate as this is a parameter under investigation. Bankoff and Han also assumed an initial condition of zero vapour volume but this causes computational difficulties (which could be avoided), and does not seem to be physically sensible. In the present work the initial volume fraction of vapour was specified by assuming an initial vapour film thickness and determining the vapour volume fraction from

$$\alpha_v = \alpha_m\left[\left(1 + \frac{2\delta}{D_p}\right)^3 - 1\right] \qquad (20)$$

where equation (20) was obtained by multiplying the volume of vapour around one particle by the number of particles per unit volume. The initial vapour film thickness was chosen as a parameter but some calculations were carried out using the following equation for the vapour film thickness obtained from reference 7,

$$\delta = 2\left[\frac{k_v \mu_v D_p (T_m - T_{sat})}{\rho_v(\rho_l - \rho_v)\, g\, h_{fg}}\right]^{1/4} \qquad (21)$$

The vapour film thickness predicted by the above equation varied from 0.33mm at 0.1MPa to 0.20mm at 6MPa for a melt diameter of 10mm and a melt temperature of 3500K. It is thought that this film thickness is too small, as the film boiling model has the same form as that of the Bromley model [19], which makes similar assumptions to those questioned in section 3.4.

Equation 16 could also have been used to obtain an estimate of the initial vapour film thickness. However, since equation 16 involves the liquid velocity it would not be possible to obtain an initial estimate of the vapour film thickness before obtaining the liquid velocity. Thus an iterative technique would have had to be employed to calculate consistent starting values for the liquid velocity and vapour film thickness. This was not considered worthwhile, due to the limitations of this film boiling model described in section 3.4.

Bankoff and Han do not state explicitly what initial velocities they used in their calculations, but because the model is for a steady-state situation the terminal velocities seem to be the appropriate choice. Initially, it was decided to make physically sensible guesses for the vapour and liquid velocities. However, this proved to be inadequate as it caused the equations to be unstable at z=0 in some circumstances, and the solution was completely dominated by a

particular drag term in others. To overcome these problems it was decided to start the calculation off with no net force acting on either the liquid or the vapour. This was achieved by solving equations (8) and (9) simultaneously with the spatial derivatives and evaporation mass flux set to zero. This proved to be a much better initial condition, as any dispersion which the model predicted was then caused by vapour production.

3.7 Solution procedure

The equations were solved using a variable order, variable step Gear method from the NAG subroutine library [20]. This proved to be very robust with the initial conditions described above. It was found that as the volume fraction of particles approached zero the calculation was likely to produce volume fractions outside the range of 0 to 1. At this point the calculation was halted. The melt volume fraction at this point was typically less than 0.01. The z value at this point was used to define the distance from the melt front at which the melt could be defined as completely dispersed. These calculations are for a steady-state situation, so that the time taken for dispersion cannot be determined and it is only possible to determine the spatial variation of the mixture components.

3.8 Model validation

The model described so far only differs from the model used by Bankoff and Han in that the evaporation reaction force acts on the vapour rather than the liquid, and the initial conditions for the velocities may be different since these were not precisely documented by Bankoff and Han. Comparison of results from the present model with those of Bankoff and Han showed them to be in good agreement, suggesting that same initial conditions were being used. The calculations of Bankoff and Han terminated at positions similar to those obtained from the present model. Thus it was concluded that the model was working correctly.

4 MODEL RESULTS

In this section the results obtained from the model as formulated by Bankoff and Han, except for the minor modifications noted in the previous section, are presented and the effects of varying the initial conditions are examined. The water properties were obtained from steam tables [21] and the properties of the uranium dioxide melt were obtained from reference [22]. A constant melt temperature of 3500K was assumed in all the calculations. A melt emissivity of 0.8 was used in all the calculations, since it is the appropriate value for uranium dioxide at 3500K [22].

Two types of initial conditions were used. In the first option, corresponding to an ISTART value of 0, the initial velocities and the volume fractions of vapour and melt were specified. In the second option, corresponding to an ISTART value of 1, both the vapour and liquid were taken to be at their "terminal velocity" and a vapour film thickness and volume fraction of melt were specified. In the next four sections the effect of ambient pressure, initial vapour film thickness, initial melt fraction, and melt particle size will be examined.

4.1 The effect of pressure

Figures 2, 3 and 4 show calculations for saturation pressures of 0.1, 1.0, and 6.0MPa respectively. An initial melt volume fraction of 0.4, a vapour film thickness of 1mm, and a particle size of 10mm were used in all the calculations. An adjustment for the effect of ambient pressure on the initial vapour film thickness was not made, as no suitable correlation could be found.

The figures show that dispersion of the melt occurs over a very short distance from the melt front. At a pressure of 0.1MPa the melt is completely dispersed within 10mm and 75% of the coolant phase is vapour. As the pressure is increased the dispersion is decreased, but the effect is relatively insignificant. At 6MPa the melt is dispersed within 60mm of the front and again 80% of the coolant is

vapour at this stage. The variation of dispersion with pressure is due to the effect of pressure on the density of steam, which varies from 0.6 kg/m^3 at 0.1MPa to 30 kg/m^3 at 6MPa. Thus the greater volume of steam produced at lower pressures causes the melt to be swept further apart. This trend of reduced dispersion with increased pressure has been observed experimentally [23].

4.2 The effect of initial vapour fraction

Figure 5 shows the result of a calculation where the intial vapour film thickness was 0.01mm, so that the initial vapour volume fraction was practically zero. Comparison with figure 3 shows that reducing the initial vapour film thickness to almost zero has only a slight effect on the melt dispersion but it changes the liquid fraction significantly.

Increasing, the vapour film thickness has a different effect. Figures 6 and 7 show the results of calculations using vapour film thicknesses of 1.6mm and 1.7mm respectively. For the case of a 1.6mm vapour film the dispersion occurs in about twice the distance of that predicted for a 1mm film. Increasing the vapour film thickness by a further 0.1mm causes completely different behaviour. The melt starts to disperse but then the melt fraction increases until all the liquid has been vaporised at a melt fraction of 0.42 and the solution procedure was halted. The dramatic difference between the solutions for vapour films of 1.6mm and 1.7mm suggests that the model is not giving physically sensible results. The small change in the vapour film thickness changes the initial liquid velocity by only 0.01m/s, but almost doubles the vapour velocity from 4.44 to 8.17m/s. Thus the drag of the vapour on the liquid is increased by a factor of 4.

The reason for the unphysical results is probably because the liquid is no longer the continuous phase, so that the drag correlations are no longer appropriate. The effect of making the vapour the continuous phase will be examined later. The above calculations suggest that the model predictions of dispersion are insensitive to

the assumed vapour fraction provided that it is sufficiently small for the liquid to be the continuous phase. However, the choice of initial vapour film thickness is crucial if the liquid volume fractions are to be meaningful.

For the range of initial vapour fractions considered the initial liquid velocity (which would correspond to the melt front velocity in a fixed frame of reference) varies from 1.06 to 1.12m/s. Thus it is not possible to determine the initial vapour fraction from experimental results, since the most easily measured parameter is insensitive to changes in the assumed vapour fraction.

4.3 The effect of initial melt fraction

The initial melt volume fraction is unlikely to be as high as 0.4, due to the large quantities of steam produced at the melt front. Figure 8 shows the results from a calculation carried out with an initial melt fraction of 0.2. Comparing this with Figure 3, which gives the results for an initial volume fraction of 0.4, shows that the melt is dispersed within a similar distance in both situations, but increasing the initial melt fraction increases the rate of dispersion with distance. This is because when there are more particles per unit volume, more vapour is produced, and the dispersion is faster. Also reducing the initial volume fraction of melt increases the amount of liquid present, but dispersal of the melt is so rapid in both cases that this is unimportant.

4.4 The effect of melt particle size

The effect of melt particle size is examined in detail in the original paper by Bankoff and Han. Figures 9 and 10 show the results from calculation using a 0.1m particle size for ambient pressures of 0.1 and 6.0MPa respectively. The figures show that increasing the particle size from 10mm to 100mm reduces the dispersion considerably, and substantially larger regions of coarse mixture are predicted. This is because of the decrease in vapour production, due to the decreased melt surface area per unit volume. However, it is doubtful

whether such large particles could be efficiently fragmented in a steam explosion [31].

5 MODIFICATIONS TO THE SEPARATED FLOW MODEL

In this section significant modifications to the model will be made to examine the sensitivity of the model to some of the assumptions made by Bankoff and Han. The radiation heat transfer model will be modified to allow for the spectral variation of the absorption length of water. A lower bound conduction model will be described as an alternative to the forced convection film boiling model. The effect of making the vapour, rather than the liquid, the continuous phase will be examined. In section 5.4 results obtained using a simple breakup model will be described. In the final section the validity of the assumption of a constant melt temperature will be examined.

5.1 A modified radiation heat transfer model

The radiation model used by Bankoff and Han in which all the radiation emitted by melt particles is absorbed by coolant is too simplified. In reality "self-heating" between melt particles when all the radiation is not absorbed by the fluid phase must be taken into account. This is not easy to do since the radiation absorption lengths in water and steam are wavelength dependent. In addition the absorption length in steam is a function of pressure and the absorption of radiation by steam causes it to be superheated. Appendix 1 examines the importance of allowing for the absorption length of the water and calculates some approximate values for the absorption of radiation by steam.

A modified radiation model was constructed in which the absorption of radiation by water (but not by steam) was properly calculated but in which the radiation not absorbed by the water was not used to produce "self heating". A characteristic liquid dimension was calculated using

$$D_l = D_p \left(\frac{\alpha_l}{\alpha_m}\right)^{1/3} \qquad (22)$$

At each space step the radiation heat flux was multiplied by the fraction of the energy which could be absorbed in the coolant length-scale given in equation (22). A simple look-up table was constructed from the results given in Appendix 1 to save computational time. Figure 11 shows the result of a calculation carried out for the same conditions as for figure 3, except that the modified radiation model was used. The figure shows that the effect is to decrease the dispersion slightly. The effect is only slight because the coolant fraction is relatively large, and so the radiation path-length through the water is relatively long. The calculation shown in figure 12 is the same as that given in figure 7, where there is a low initial liquid fraction, except that the modified radiation model was used. In this case the figure shows that the dispersion is affected significantly.

It is not possible to model the "self-heating" effect of radiation on the melt since a fixed temperature is assumed for the melt particles. To allow for heat transfer correctly it would be necessary to allow for the reduction in melt temperature with time. This could be very important since the radiation heat flux varies as the fourth power of the melt temperature but the "self-heating" effect would slow down the rate of cooling of the melt. In a time-dependent model it would also be possible to construct an energy equation for the vapour, to allow for the superheating of the vapour. This would be due to both conduction and convection from the melt, and the absorption of thermal radiation. The latter effect is small at low pressure but increases with pressure as detailed in Appendix 1. Thus it does not seem possible to improve the modelling of the radiation heat transfer further without adopting a time dependent model.

5.2 An alternative film boiling model

The correct way to model the vapour conduction and convection heat transfer is far from obvious. Clearly a convective heat transfer coefficient for the case of gas flow past a sphere would be more appropriate than a forced convection film boiling correlation when virtually no liquid is present. Again it would be important to allow for the superheating of the vapour in this situation.

Also at the very high temperature occuring within the mixture the dissociation of steam becomes important. Observed values of 13% dissociated at 3000K, 0.1 MPa are given in reference 24. The fraction of steam dissociated increases with temperature to 30% at 3500K, 0.1MPa. The effect of increasing the ambient pressure is to reduce the dissociation to 15% at 3500K, 1.0 MPa. The hydrogen produced in this process can increase the thermal conductivity of the vapour by several orders of magnitude [25]. Table 1 below shows the effect of pressure and temperature on the thermal conductivity of dissociated steam. The data was taken from reference 25.

	Pressure (MPa)		
k (W/m K)	0.1	1.0	6.0
Temperature (K)			
saturation	0.025	0.034	0.058
1400	0.187	0.186	0.186
2400	0.690	0.469	0.396
3400	6.270	2.600	1.450

Table 1: The effect of pressure and temperature on the thermal conductivity of dissociated steam

In the present model the vapour remains at its saturation temperature which cannot be valid when the liquid fraction becomes low.

A lower bound on the conduction heat transfer was set by using equation 20 to determine an effective vapour film thickness from the

volume fraction data, and then setting the heat transfer coefficient equal to the thermal conductivity of saturated vapour divided by the vapour film thickness. Figure 13 shows a plot obtained by using the model for the same conditions as those used in figure 11 and shows a slight increase in the region over which a mixture exists. Comparison with figure 3 shows that modifying both the radiation and the film boiling models approximately doubles the size of the mixture region. However, both heat transfer models are very sensitive to the assumed vapour fraction.

5.3 Changing the continuous phase

As the volume fraction of steam increases it is no longer possible to assume that the continuous phase is the liquid. Changing the continuous phase requires the modification of the drag terms in the momentum equations. In this situation the drag of the liquid on the particles is set to zero, and only the drag of the vapour on the melt and water globules has to be calculated. The diameter of the water globules was obtained from equation 22. The appropriate drag coefficient was obtained from reference 12 and is given by

$$C_D = 0.45 \left[\frac{1 + 17.67(1 - \alpha_d)^{93/35}}{18.67(1 - \alpha_d)^{3.1}}\right]^2 \qquad (23)$$

The drag terms were then constructed using equation (12). Because the vapour is the continuous phase, the drag force is proportional to the vapour density rather than the liquid density. This reduces the drag forces considerably, and thus should reduce the dispersion. The same starting options were used, except that the modified drag terms were used to calculate the "terminal velocities".

Figure 14 shows the result of a calculation where the continuous phase is the vapour. The initial conditions are the same as those for figure 12. The figure shows that there is considerably less

dispersion, with the melt fraction greater than 0.2 at 0.1m from the front. However, the starting velocities are unphysically large, with a vapour velocity of 12m/s and a liquid velocity of 20m/s. This is because the melt at the leading edge is falling at its terminal velocity through steam rather than liquid coolant. The initial velocities obtained when a liquid continuous phase was assumed are much closer to those observed experimentally. This suggests the following picture; melt falling through water with a spatially rapid transition to a vapour continuous phase above the falling front.

Figure 15 shows the result of a calculation where the initial conditions are those appropriate to a continuous phase of water but subsequently the continuous phase is steam. The result is a sudden change in the volume fractions above the melt front followed by a deep region of slowly increasing dispersion. In reality there would be a gradual change of continuous phase which would smooth out the transition. It is not clear how this can be modelled but it is clearly an important feature. When the vapour is the continuous phase fluidization of the melt and liquid coolant can occur. The position at which the fluidization velocities occur will depend on the complex variation of the coolant phase in the region of the melt front.

5.4 Modelling the breakup of melt and coolant

Breakup of the droplets of melt and coolant is a transient process and cannot be modelled correctly in a steady-state model. Various correlations for the rate of melt breakup exist. A simple model based on exponential decay of the particle size with time has been used by Corradini to model the FITS data [7,8]. The stability of a drop to breakup by inertial forces is determined by a critical Weber number, with breakup occurring for

$$\frac{\rho_v (u_d - u_v)^2 D_d}{\sigma} > We_{crit} \qquad (24)$$

where the critical Weber number, obtained from experimental data, is typically 7-12 [6].

A series of calculations was made where the particle diameter for both the melt and the liquid coolant was determined by ensuring that the Weber number was always less than or equal to the critical Weber number. A calculation was made where the initial conditions were the same as those used for Figure 15 and a critical Weber number of 12 was used. The melt dispersion in the two cases was very similar but the melt particle size was reduced from 10mm initially to 6mm after 0.1m. The coolant length was reduced from 5mm to 0.7mm. In this case the extra vapour generation caused by the smaller melt particles seems to have been balanced by the reduction in vapour generation, due to a reduction in the amount of radiation absorbed in the smaller water globules, and the change in the drag forces due to the change in particle size.

Figure 16 shows the results of a calculation using a critical Weber number of 7. In this case the melt dispersion is increased, showing that the critical Weber number is an important parameter. This breakup of the coolant would be even more important if the vapour was superheated, since the greater surface area would lead to more evaporation. The liquid velocity shows a completely different behaviour from the case where there was no fragmentation. For the case of no breakup the liquid velocity decreases monotonically from 1m/s to 0.08m/s after 0.1m. When breakup was modelled using a critical Weber number of 12, the velocity increased to 1.5m/s after a distance of 0.05m and then slowly decreased to 0.9m/s at 0.1m. Similar behaviour was observed for a critical Weber number of 7. This different behaviour is caused by the change in the drag terms. As the liquid is fragmented there is a greater drag on it by the steam (due to the increased projected area) and thus its velocity increases. There is also reduced steam production due to the decreased absorption of thermal radiation.

The results presented in this section have assumed the continuous phase to be the vapour. The results show that the breakup of the liquid water is as important as breakup of the melt. Thus it is important to allow for coolant breakup if the model is to be capable of predicting coolant fluidization, as both the particle size and velocity depend on the breakup mechanism. A time dependent model is needed to investigate fluidization, since a steady-state model can only show the end state of the mixing process and does not allow the quantity of coolant which has been removed from the mixing vessel to be determined; but the present results confirm the work of Corradini and Moses [36] who noted the importance of allowing for coolant breakup in fluidization calculations. In the original model of Bankoff and Han the continuous phase was the liquid, so that in this case only melt breakup could occur, and coolant fluidization is not possible. This again emphasises the need to choose the correct continuous phase, since an incorrect choice rules out possibly important mechanisms. The above comparison shows how breakup can be incorporated into the steady-state model. With a time dependent model it would be possible to model a breakup time.

5.5 Validity of the assumption of a constant melt temperature

Bankoff and Han assumed that all the radiation emitted by the melt was absorbed by the coolant. For a melt emissivity of 0.8 and a melt temperature of 3500K this gives a heat transfer coefficient of 1600 W/m^2K. The table below shows the surface temperature and fractional energy release for a 10mm melt sphere for the above conditions.

Time (ms)	Fractional Energy Release	Surface Temperature (K)
0	.0000	3500
50	.0110	3193
100	.0205	3074
150	.0300	2985
200	.0393	2911
300	.0571	2793
500	.0907	2613
700	.1219	2474
900	.1513	2359

Table 2: Heat transfer from a 10mm sphere of melt radiating to an infinite pool

The above results were calculated using a distributed heat diffusion model, assuming all properties remained constant and neglecting the latent heat released upon freezing. The model is fully described in reference 10. The freezing point of uranium dioxide is 3120K [22]. Thus the above calculation shows that the outer surface of the melt starts to freeze after about 70ms. The above results also show that:

(i) It is not possible to assume a constant melt surface temperature and at the same time assume a high radiation heat flux. The "self heating" effect described in section 5.1 would reduce the heat transfer coefficient and modify this result. The radiation heat flux is proportional to the fourth power of the absolute temperature, so that any allowance for the cooling of the melt would reduce the radiation heat flux considerably.

(ii) The concept of a mixture developing over timescales approaching a second requires that the surface heat transfer coefficient of the melt to be low. For h=1000 W/m^2K, freezing starts after about 170ms and for h=500 W/m^2K, freezing starts after about 640ms. Thus if the melt is to remain molten, to allow fragmentation to occur, heat transfer rates within the mixture must be very low. This would be

the case if the mixture consisted of only melt and vapour. In this case heat would only be lost around the edge of the mixture and most of the radiation emitted by a melt particle would be absorbed by other particles. It is not possible to determine the crust thickness using the present heat transfer model because it does not allow for the latent heat released as the melt freezes.

A mixture is often thought of as being a collection of melt particles, each surrounded by a thin vapour blanket, in a pool of coolant. The calculations obtained from the modified mixing model suggest that this configuration may not be possible due to the rapid vaporisation of the coolant between the melt. Indeed if the above picture were correct radiation heat transfer and convective film boiling heat transfer would be effective and the melt would rapidly freeze. The combination of these results suggests there must be very little water present in a mixture so that most of the radiation emitted by the melt causes "self heating". In this case the assumption of a constant melt temperature would seem to be justified.

6 COMPARISON OF THE HOMOGENEOUS AND SEPARATED FLOW MODELS

So far all the calculations have been made using a separated flow model. Bankoff and Han compared the results from a homogeneous flow model with those from a separated flow model and concluded that they were very similar. They have subsequently developed a one-dimensional unsteady model and a two-dimensional unsteady model using a homogeneous two phase flow model. It is thus important to determine whether use of the simpler model can be justified. In this section results obtained using a homogeneous model are compared with those obtained from the separated flow model. The model equations are derived in Appendix 2.

Figures 17, 18 and 19 show the results of computations carried out for the same conditions as those used for figures 2, 3 and 4, which were produced from the separated flow model. Again it can be seen that increasing the

ambient pressure reduces the dispersion. Comparison of the figures shows that the dispersion is very similar at ambient pressure, but that the dispersion is less rapid in the homogeneous flow model for higher pressures, with a region of 0.1m in the homogeneous flow case in which the melt fraction was greater than 0.1 at 6MPa, compared with 0.05m in the separated flow case.

Figures 20 and 21 show the effect of varying the fluid velocity at the melt front for a pressure of 1.0MPa. The figures show that this has a very significant effect on the rate of dispersion, with the melt completely dispersed within 20mm for an initial velocity of 2m/s compared with a region of mixture of the order of 100mm for an initial velocity of 0.5m/s. Thus the predicted results are extremely sensitive to the choice of initial fluid velocity.

Figure 22 shows the results from a calculation where the initial void fraction was 0.8. Comparison with figure 18, where the initial void fraction was zero, shows that the dispersion is less rapid for a higher void fraction. This is because the drag force is proportional to the fluid density, which varies according to the fraction of liquid and vapour present. Because of this the initial fluid velocity is increased from 1.06m/s to 2.45m/s for a change of vapour fraction from zero to 80%. In this model the fluid is the continuous phase and a weighted density is used to determine drag forces. There is no need to model a transition from a continuous phase of liquid to one of vapour, although the drag coefficient should be changed. However, because the liquid density is about 1600 times that of the vapour (at ambient pressure) the fluid density, and consequently the drag force, remains high even when the fluid is composed almost entirely of vapour. The same effect would cause the predicted Weber numbers to be large and thus would cause too much fragmentation of the melt. Because there is assumed to be no slip between the liquid and vapour this model cannot be used to examine coolant fluidization, as the water is always carried out with the vapour.

In summary, the separated flow model is preferred since although both the models predict rapid dispersion of the melt, the predictions for other

variables are very different. Because the homogeneous flow model assumes there to be no slip between the liquid and vapour phases it cannot be used to explore important physics, such as coolant fluidization and breakup of the liquid or melt by the flow of vapour.

7 CONCLUSIONS

(i) The unmodified one-dimensional steady-state flow model of Bankoff and Han usually gives dispersion of the melt by steam in very short distances. Typically, if the melt is assumed to be in 10mm spheres the region of mixture at ambient pressure is only of the order of 10mm. This is increased to about 60mm for a pressure of 6MPa.

(ii) The model predictions were found to be very sensitive to the assumed initial vapour fraction. In some cases, if this was large enough, a region of melt accumulation was predicted. These predictions are not thought to be physically correct, as in this case the assumption of a continuous liquid phase seems to be invalid.

(iii) The validity of the assumed heat transfer models has been questioned. A detailed examination of radiation heat transfer has shown that the absorption of thermal radiation by water is not complete, due to the shift of the radiation spectrum towards lower wavelengths for high temperature melts. A correction for this has been made and was found to reduce the amount of radiation absorbed by typically 50%. A simple modified film boiling model has also been used to set a lower bound on conduction heat transfer. Both modifications have reduced the predicted dispersion.

(iv) Calculations have been carried out for the case of a continuous phase of vapour rather than liquid. This has reduced the dispersion considerably and seems physically more reasonable when typically 80% of the fluid is in vapour form. Calculations of the velocity of the leading edge of the mixture suggest that the continuous phase is initially water but that it changes to vapour above the front, due to the generation of large volumes of vapour.

(v) A simple breakup model has also been implemented and it has been shown that it is important to model breakup of the melt and coolant if fluidization limits are to be predicted correctly. The effect of melt and coolant breakup on melt dispersion was found to depend on the value chosen for the critical Weber number. With a critical Weber number of 12 the dispersion was not significantly affected by breakup but for a critical Weber number of 7 the dispersion was increased.

(vi) It is shown that if there is a substantial fraction of liquid coolant present the heat transfer rate is high enough to cause rapid freezing of the melt. All the present calculations suggest that there is relatively little water in a mixture if the melt is at a temperature of 3500K, so that in this case the melt does not freeze because the net heat transfer rate from the melt is small.

7.1 Recommendations

(i) There is still a need for a better understanding of the physics of coarse mixing. Detailed information about the internal composition of a mixture is needed so that the correct physical processes can be identified. It is hoped that the WUMT experiments being carried out at AEE Winfrith will provide some of this information [9].

(ii) Bankoff and Han have produced two further models. The first is again one-dimensional but is unsteady [29], and the second is unsteady and two-dimensional [30]. Both modifications are based on the homogeneous flow model described in this paper and both use the heat transfer models questioned in this paper. The two-dimensional model allows the radial expansion of the mixture to be modelled and would be useful for analysis of the WUMT experiments. The extension of the present set of equations to the two-dimensional unsteady situation is relatively simple. However, it is much more difficult to solve the set of partial differential equations which result. In future work it would seem sensible to concentrate on the separated flow model, rather than the homogeneous flow model, for the reasons

given in section 6. In addition the dynamic models could then be used to examine the validity of the fluidization limits suggested by Corradini [36].

(iii) It would be useful to construct extra energy conservation equations to allow the importance of melt cooling and vapour superheating to be examined.

ACKNOWLEDGEMENT

The author would like to thank Dr J B Knowles of AEE Winfrith for suggesting the importance of allowing for the spectral absorption of radiation and the dissociation of steam.

REFERENCES

1. Bankoff, S G, and Han, S H, Mixing of molten core material and water. Nuc Sci and Eng, 85, p.387-395. (1983)

2. Report on PWR Degraded Core Analysis. Edited by J H Gittus. UKAEA report NDR-610(s), Chapter 5 (1982)

3. Briggs, A J, The probability of containment failure by steam explosion in a PWR. AEEW-R1692 (1983)

4. Board, S J, Hall, R W and Hall, R S, Detonation of fuel coolant explosions. Nature, 254, p.319-321. (1975)

5. Henry, R E, and Fauske, K H, Required initial conditions for energetic steam explosions. Paper presented at ASME winter meeting, Washington. (1981)

6. Corradini, M L, A proposed model of fuel-coolant mixing. Trans Am Nucl Soc, 41, p.415-416. (1982)

7. Corradini, M L, and Moses, G A, A dynamic model of fuel coolant mixing. Presented at the International meeting on light water reactor severe accident evaluation, Cambridge, Massachusetts. (1983)

8. Corradini, M L, Molten fuel/coolant interactions: Recent analysis of experiments. Nucl Sci and Eng, 86, p.372-387. (1984)

9. Fletcher, D F, A description of fractional factorial experimental design and its application to the Molten Fuel Test Facility. AEEW-M2178 (1984)

10. Fletcher, D F, Modelling the transient energy release from molten fuel coolant interaction debris. AEEW-M2125 (1984)

11. Fletcher, D F, A review of hydrodynamic instabilities and their relevance to mixing in molten fuel coolant interactions. AEEW-R1758 (1984)

12. Ishi, M, and Zuber, N, Drag coefficient and relative velocity in bubbly, droplet and particulate flows. AIChE, 25, p.843-855. (1979)

13. Witte, L C, Film boiling from a sphere. I & E C Fundamentals, 7, p.517-518. (1968)

14. Sparrow, E M, and Cess, R D, Radiation heat transfer. Hemisphere publishing corporation, Washington. (1978)

15. Pearson, K G, and Elliott, D, The absorption of thermal radiation by water films. AEEW-R1098. (1977)

16. Curico, J A, and Petty, C G, The near infrared absorption spectrum of liquid water. J. Opt Soc Am, 41, p.302-306. (1951)

17. Wallis, G B, One-dimensional two phase flow. Mc-Graw Hill. (1969)

18. Nguyen, H, One dimensional models for transient separated two-phase flow. Paper in proceedings of third CSNI specialists meeting on transient two phase flow, Edited by M S Plesset, N Zuber and I Cotton, Hemisphere publishing company. (1983)

19. Bromley, L A, Heat transfer in stable film boiling, Chem Eng Prog, 46, p.221-227. (1950)

20. Numerical Algorithms Group Subroutine Library, routine DO2EBF.

21. U.K. Steam tables in S.I. units Arnold, London. (1970)

22. Fink, J K, Chasanov, M G, and Leibowitz, L, Transport properties of uranium dioxide ANL-CEN-RSD-80-4 and Thermodynamic properties of uranium dioxide ANL-CEN-RSD-80-3. (1981)

23. Bird, M J, An experimental study of scaling in core melt/water interactions. Presented at the 22nd National Heat Transfer Conference, Niagara Falls, 5-8 August, 1984

24. Dorsey, N E, Properties of ordinary water substance, Hafner Publishing Company, New York (1968)

25. Vangajtik, N B, Tables of the Thermophysical properties of liquids and gases. Hemisphere Publishing Company. (1975)

26. Sharon, A, and Bankoff, S G, Propagation of shock waves through a fuel/coolant mixture part 1: Boundary layer stripping mechanisms. In Topics in two-phase heat transfer and flow, Ed. by S G Bankoff, ASME, New York. (1978)

27. Two-phase flow and heat transfer. Edited by D Butterworth and G F Hewitt, O.U.P. (1977)

28. Numerical Algorithms Group Subroutine Library, routine D02BBF

29. Bankoff, S G, and Han, S H, An unsteady one-dimensional two-fluid model for fuel-coolant mixing in an LWR meltdown accident. Presented at the US-Japan seminar on Two-phase flow dynamics, Lake Placid NY, July 29-August 3, 1984

30. Bankoff, S G, and Hadid, A, The application of a user-friendly code to nuclear thermal hydraulic reactor safety problems. Presented at the International Nuclear Power Plant Thermal Hydraulics and Operations Meeting in Taipei, Taiwan, ROC, October 22-24, 1984

31. Fletcher, D F, A review of coarse mixing models. CLM-R251 (1985)

32. Kreith, F, Principles of heat transfer. Harper and Row, New York. (1976)

33. Fry, C J, and Robinson, C H, Results from selected experiments performed in the THERMIR facility at AEE Winfrith. AEEW-M1778 (1980)

34. Robertson, C W, and Williams, D, Lambert absorption coefficients of water in the infrared. J Opt Soc Am, 61, p.1316-1320. (1971)

35. Welty, J R, Wilson R E, and Wicks, C E, Fundamentals of momentum, heat and mass transfer. Wiley and Sons, New York. (1976)

36. Corradini, M L, and Moses G A, Limits to fuel/coolant mixing. Nucl Sci & Eng, 90, p.19-27 (1985)

37. Hale, G M, and Querry, M R, Optical constants of water in the 200-nm to 200 micron wavelength range. Applied Optics, 12, p.555-563. (1973)

38. Fox, J J, and Martin, A E, Investigations of infra-red spectra (2.5-7.5 microns) absorption of water, Proc Roy Soc, 174, p.234-262. (1940)

39. Hale, G M, Querry, M R, Rusk, A N, and Williams, D, Influence of temperature on the spectrum of water. J Opt Soc Am, 62, p.1103-1108. (1972)

40. Collins, J R, Data referenced in Table 162 of reference 24.

41. Irvine, W M, and Pollack, J B, Infrared optical properties of water and ice spheres. ICARUS, 8, p.324-360. (1968)

42. Popov, Y A, and Shvartsblat, R L, IR absorption coefficients and refractive indices of carbon dioxide and steam. High Temp (USA), 12(6), p.1047-1050. (1974)

43. Hottel,, H C, and Egbert, R B, Radiant heat transmission from water vapour. AIChE Trans. 38, p.531-568 (1942)

44. Ferriso, C C, Ludwig, C B, and Thomson, A L, Empirically determined infrared absorption coefficients of water from 300 to 3000K. J Quant Spectrosc Radiat Transfer, 6, p.241-273 (1966)

APPENDIX 1: RADIATION HEAT TRANSFER TO STEAM AND WATER

A1.1 INTRODUCTION

In this appendix the radiation heat transfer from high temperature melts to water and steam is examined. The absorption coefficients in water and steam are wavelength dependent and so the fraction of thermal radiation absorbed is calculated as a function of melt temperature for given water and steam thicknesses. The absorption coefficient is also dependent on the coolant pressure and temperature and so the fraction of incident radiation absorbed as a function of water and steam thickness is calculated for various coolant temperatures and pressures.

A1.2 THE BLACKBODY RADIATION SPECTRUM

A blackbody is a body which emits and absorbs, at any temperature, the maximum possible amount of radiation at any given wavelength. Thus the assumption of a blackbody gives the upper bound on the amount of energy that can be absorbed or transmitted by radiation. The spectral distribution of energy emitted by a blackbody per unit area per unit time was derived by Planck and is given by [32]:

$$W = \frac{2\pi c^2 h\ \lambda^{-5}}{\exp(ch/k\lambda T)-1} \qquad \text{(A1.1)}$$

where: k=Boltzmann constant = 1.38E-23 J/K
c=speed of light = 3.0E8 m/s
h=Planck's constant = 6.6E-34 J/s

In reality the amount of radiation emitted and absorbed by a body is less than this upper bound. If the ratio of the amount of radiation which is actually absorbed to the amount which could ideally be absorbed is approximately constant over all wavelengths the body is said to be gray, with the above ratio termed the emissivity. This is a good approximation for many materials [32], but water is an important exception. The

variation of absorption of radiation with wavelength will be examined in detail in the next section.

Figure A1 shows the effect of temperature on the spectral energy distribution for three temperatures appropriate to coarse mixing studies. Many experiments have been carried out using simulant materials [33], such as aluminium, where the melt temperature is approximately 1000K. Experiments carried out at the Sandia National Laboratories use iron-alumina thermites, which are at a temperature of about 2500K during mixing [8]. Finally, experiments at AEE Winfrith use uranium dioxide/molybdenum thermites which are at a temperature of 3500K [23]. The figure shows that increasing the melt temperature has two effects:

Firstly, increasing the melt temperature increases the amount of energy transferred by radiation. Integrating equation (A1.1) over the entire range of wavelengths gives

$$q/A = \sigma T^4 \qquad \text{(A1.2)}$$

where: q/A= Heat transfer rate per unit area
σ= Stefan-Boltzmann constant =5.67E-8 W/m^2K^4
T= Temperature K

Equation A1.2 gives the well-known result that the amount of energy transferred by radiation varies as the fourth power of the absolute temperature. Table A1 below shows the value of radiation heat flux for the above temperatures.

T (K)	q/A (MW/m^2)
1000	0.057
2500	2.2
3500	8.5

Table A1: The effect of melt temperature on radiation heat transfer.

The above results show that the energy transferred by radiation is very small for the low temperature melts but that the radiation heat transfer rate is extremely large for high temperature thermite generated melts. Thus it is very important to model radiation heat transfer correctly when considering high temperature melts.
Secondly, as the temperature is increased more of the energy is in the shorter wavelength range. At 3500K the melt is incandescant due to the large fraction of the energy which is present in the visible range (0.4-0.7μm). Thus it is important to determine how effective water is at absorbing thermal radiation in various wavelength ranges.

A1.3 THE ABSORPTION OF THERMAL RADIATION BY WATER

The amount of radiation absorbed by a layer of water depends both on the thickness of the water layer and on the spectral distribution of the incident radiation. It has been found experimentally that the amount of radiation of wavelength λ absorbed in a distance z is given by

$$W_{\lambda z} = W_{\lambda o}\left(1 - \exp(-\alpha_\lambda z)\right) \qquad (A1.3)$$

where $W_{\lambda o}$ = the amount of radiation incident per unit area per unit time

z = path-length of the radiation

α_λ = spectral absorption coefficient

The above law is often referred to as Lambert's law and α_λ is called variously, the Lambert absorption coefficient, the absorption coefficient or the monochromatic absorptivity. The reciprocal of the absorption coefficient gives the length of water required to be traversed to reduce the intensity by a factor of 1/e. This distance is often termed the absorption length. The absorption coefficient can also be obtained from the imaginary part of the refractive index, n', and is given by

$$\alpha_\lambda = 4\pi n'/\lambda \qquad (A1.4)$$

The data used in this investigation was obtained from references 16 and 34. These experimental investigations covered the wavelength ranges of 0.7 to 2.5 microns and 2.326 to 33.33 microns respectively. In the experiments of reference 16 the water was at 20°C and ambient pressure. In the second reference the conditions are not stated but the description of the experiments suggests that the conditions were also ambient temperature and pressure.

Figure A2 shows a plot of the absorption coefficient against wavelength for a wavelength range of 0.7 to 32 microns. Over this range the absorption coefficient varies by over 6 decades. The variation in absorption length is from one metre to one micron. Figure A3 gives a detailed plot for the wavelength range of 0.7 to 9 microns. The plot shows that there are seven prominant absorption bands in this range. These bands are relatively narrow, so that care must be taken when determining how much energy is absorbed in each band.

Figure A4 shows the distribution of emissive power as a function of λT. The data for the plot was obtained from reference 35, which gives a table of values for the integrated emissive power over various wavelength ranges. Thus given a melt temperature figure A4 can be used to determine the fraction of the emissive power in various wavelength ranges. In particular, a quick calculation shows that about 30% of the energy of a body at 3500K is in the wavelength range zero to one micron, where the absorption length is of the order of a metre. Thus further calculations are needed to determine the amount of thermal energy absorbed as a function of path-length for various melt temperatures.

A computer program was written to integrate equation A1.3 with respect to wavelength using the absorption length data given in figures A2 and A3. This data covers a wavelength range of 0.7-33 microns. Below 0.7 microns the water was assumed to be transparent [24] and the radiative energy in wavelengths above 33 microns was found to be negligible. The trapezium rule was used with 128 data points and was found to give accurate results. Table A2 below shows the fraction of incident energy absorbed as a function of temperature and distance. The radiation emitted by the water

was ignored, since its temperature is at least one-third of that of the melt and in the case of uranium dioxide one-tenth.

PATH-LENGTH (mm)	FRACTION OF INCIDENT ENERGY ABSORBED		
	T = 1000K	T = 2500K	T = 3500K
1	0.967	.599	.343
5	1.	.707	.472
10	1.	.756	.526
15	1.	.786	.560
20	1.	.806	.585
25	1.	.822	.604
30	1.	.834	.620

Table A2: The fraction of thermal energy absorbed as a function of melt temperature and path-length

The above results show that at 1000K virtually all the thermal energy is absorbed in 1mm of water. A detailed study of the absorption of thermal radiation at this temperature can be found in reference 15. At the higher temperatures, which are more appropriate to coarse mixing, the fraction of the radiant energy absorbed in a given distance is much less. At 3500K only 34% is absorbed in the first millimetre and this figure is only increased to 62% after 30mm. Thus in a mixture of water and high temperature melt it is unrealistic to assume 100% absorption of thermal radiation.

A1.3.1 The Effect of Pressure and Temperature on the Absorption Length

There seems to be very little information available about the effect of temperature and pressure on the absorption of thermal radiation in water. Most experimental determinations have been carried out using ambient pressure and temperature conditions. Hale and Querry [37] and Irvine and Pollack [41] have performed extensive reviews of optical data for water and provide many useful references. Fox and Martin [38] have investigated

the effect of temperature for the wavelength range 2.5-7.5μm and a temperature range of 3-70°C. They found that as the temperature was increased the 3μm band moved towards lower wavelengths and the 4.7 and 6μm bands moved towards higher wavelengths. In all cases increasing the temperature decreased the absorption coefficient. A more recent study by Hale et al [39] gives the following data for three absorption bands in the infrared region.

T(°C)	λ(μm)	$\alpha_\lambda(cm^{-1})$	λ(μm)	$\alpha_\lambda(cm^{-1})$	λ(μm)	$\alpha_\lambda(cm^{-1})$
5	2.96	13415	6.10	2245	16.94	3245
27	2.95	12664	6.06	2356	17.24	3227
70	2.90	10226	6.10	2204	19.60	2754

Table A3: The effect of temperature on absorption length

The data shows similar trends to that of Fox and Martin [38]. An increase in the temperature of 60°C decreased the absorption coefficient by about 25% for the band at 2.95μm. They also found that the width of the absorption band at half its maximum height did not vary significantly with temperature.

There is insufficient data available to determine in detail how the absorption of thermal radiation varies with coolant temperature. All the results found show that increasing the water temperature decreases the absorption coefficient. However, the absorption length is so short for the bands examined experimentally that even if it were increased by two orders of magnitude it would still only be of the order of hundreds of μm. Thus it is thought that increasing the coolant temperature would not make any significant change to the fraction of thermal energy absorbed by coolant zones with a length scale of the order of millimetres, for temperatures appropriate to coarse mixing.

There is even less data available on the effect of pressure on the spectral absorption coefficient. Experimental results of Collins [40] suggest that an increase in the pressure from 120 to 5000 bars produced no

change in the absorption coefficient of water for the wavelength range 0.71-1.05μm. No other data could be found.

A1.4 THE ABSORPTION OF THERMAL RADIATION BY STEAM

There seems to be much less data available on the spectral absorption of thermal radiation by steam. A survey of experimental data is given in references 24 and 44. Due to the very narrow absorption bands which occur experimental determination of the absorption length is very difficult [24]. In this paper the theoretical absorption coefficients determined by Popov and Shvartsblat [42] are used. Absorption coefficients are given for steam temperatures of 300K, 1000K and 2000K with the absorption coefficient being proportional to the pressure. Figures A5, A6 and A7 show the variation of the absorption coefficient with wavelength for the above temperatures. The figures show that as the steam temperature increases the absorption coefficient decreases significantly.

The method described in section A1.3 was used to examine the effect of melt temperature, vapour temperature and pressure on the fraction of the incident radiation absorbed by layers of steam of various thicknesses. Radiation by the steam has been ignored, because either its temperature is very low compared to that of the melt, or for high temperatures the emissivity of layers of steam of the thickness considered here is very low, typically 0.01 [43]

A1.4.1 The effect of Melt Temperature

Table A4 below shows the effect of melt temperature on the fraction of thermal energy absorbed by steam at a pressure of 1 bar and a temperature of 300K.

PATH-LENGTH (mm)	FRACTION OF INCIDENT ENERGY ABSORBED		
	T = 1000K	T = 2500K	T = 3500K
1.0	.009	.003	.002
2.0	.016	.006	.003
5.0	.037	.014	.008
10.0	.065	.026	.014
20.0	.106	.044	.024
40.0	.153	.067	.037
60.0	.179	.082	.047
80.0	.196	.094	.054
100.0	.209	.103	.060

Table A4: The effect of melt temperature on the fraction of the radiation absorbed by steam

The results in the above table show that as the melt temperature increases the fraction of the thermal radiation absorbed decreases. This is due to more of the thermal energy being in shorter wavelengths where the absorption coefficient is low. At 3500K only 6% of the radiation is absorbed in 100mm. Thus in the mixing application, where this likely to be an upper bound on the distance between melt particles, the absorption of thermal radiation by steam at ambient pressure can be neglected. As the melt temperature is reduced a greater fraction of the incident thermal radiation is absorbed but the total incident radiation falls rapidly with melt temperature, as detailed in Table A1.

A1.4.2 The effect of Vapour Temperature

Table A5 below shows the effect of variation of the steam temperature on the fraction of thermal radiation absorbed by layers of steam of various thicknesses, for a melt temperature of 3500K and a pressure of 1 bar.

PATH-LENGTH (mm)	FRACTION OF INCIDENT ENERGY ABSORBED		
	T = 300K	T = 1000K	T = 2000K
1.0	.002	.001	.000
2.0	.003	.001	.001
5.0	.008	.003	.001
10.0	.014	.006	.003
20.0	.024	.011	.006
40.0	.037	.021	.011
60.0	.047	.030	.016
80.0	.054	.038	.021
100.0	.060	.046	.025

Table A5: The effect of vapour temperature on the fraction of the radiation absorbed by steam

The above results show that as the steam temperature is increased the absorption of thermal radiation is decreased. For steam at 2000K and a melt temperature of 3500K, less than 3% of the incident radiation is absorbed in 100mm. During mixing there is likely to be considerable superheating of the steam in close proximity of the melt from conduction and convection, causing the steam to become even more transparent to thermal radiation.

A1.4.3 The effect of Pressure

Table A6 below shows the effect of varying the pressure on the absorption of thermal radiation by steam for a melt temperature of 3500K and steam superheated to 2000K.

PATH-LENGTH (mm)	FRACTION OF INCIDENT ENERGY ABSORBED		
	P = 0.1MPa	P = 1.0MPa	P = 6.0MPa
1.0	.000	.003	.016
2.0	.001	.006	.030
5.0	.001	.014	.064
10.0	.003	.025	.107
20.0	.006	.046	.160
40.0	.011	.080	.220
60.0	.016	.107	.257
80.0	.021	.128	.284
100.0	.025	.145	.304

Table A6: The effect of pressure on the fraction of radiation absorbed by steam

The above results show that increasing the pressure causes a considerable increase in the amount of thermal radiation absorbed. For a pressure of 6 MPa 10% of the incident radiation is absorbed within 10mm. For pressures applicable to the WUMT experiments, 1-15 bars, the steam is almost transparent to thermal radiation for the path-lengths considered here. It is only when the pressure is increased significantly that the steam can no longer be treated as transparent.

In the above calculations the pressure is due solely to the presence of steam. The effect of adding a permanent gas to change the pressure has been examined in reference 24. In the reactor safety application hydrogen or argon may be present. Although neither of these gases absorb thermal radiation they may affect the absorption properties of steam. Some information about the effect on the emissivity of adding a permanent gas to water vapour is given in reference 42. In the coarse mixing of melt and water, the water is likely to be close to its saturation temperature, so that most of the pressure is due to steam.

APPENDIX 2: DESCRIPTION OF THE HOMOGENEOUS FLOW MODEL

In this appendix the homogeneous flow model equations are derived. The same assumptions as those listed in section 2 are made. The only difference is that there is assumed to be no slip between the coolant phases, so that the liquid and vapour can be modelled as a single phase, having the following density [27]

$$\rho_f = \alpha\rho_v + (1 - \alpha)\rho_l \qquad \text{(A2.1)}$$

Conservation of mass for the melt again gives $u_m = 0$, and conservation of mass for the fluid gives;

$$\frac{d}{dz}(u_f\rho_f\alpha_f) = 0 \qquad \text{(fluid)} \quad \text{(A2.2)}$$

Conservation of momentum applied to the melt and fluid give the following equations

$$\alpha_m\rho_m u_m \frac{du_m}{dz} = 0 = -\alpha_m \frac{dP}{dz} - \alpha_m\rho_m g + F_{mf} \qquad \text{(melt)} \quad \text{(A2.3)}$$

$$\alpha_f\rho_f u_f \frac{du_f}{dz} = -\alpha_f \frac{dP}{dz} - \alpha_f\rho_f g - F_{mf} \qquad \text{(fluid)} \quad \text{(A2.4)}$$

Again the pressure gradient is eliminated from equation A2.4 using equation A2.3 to give

$$\alpha_f\rho_f u_f \frac{du_f}{dz} = \alpha_f(\rho_m - \rho_f)g - \frac{F_{mf}}{\alpha_m} \qquad \text{(fluid)} \quad \text{(A2.5)}$$

Conservation of energy applied to the fluid gives the following equation

$$\alpha_f\rho_f u_f \frac{d}{dz}(h_f + 1/2\ u_f^2) = Q - F_{mf}u_f - \alpha_f\rho_f u_f g \qquad \text{(fluid)} \quad \text{(A2.6)}$$

Introducing the quality x, which is equal to the fraction of the mass flowrate of fluid which is vapour, gives the following relations

$$h_f = h_l + x\, h_{fg} \tag{A2.7}$$

and

$$x = \alpha\, \rho_v/\rho_l \tag{A2.8}$$

Equations A2.7 and A2.8 can be used to determine a relation between the fluid enthalpy and the void fraction, which can be used to eliminate fluid enthalpy from equation (A2.6). After some manipulation, assuming the vapour to be incompressible, and using the fact that the vapour density is considerably less than the liquid density, the following equation can be derived

$$\alpha_f u_f h_{fg} \rho_v (1 + \alpha\, \rho_l/\rho_f) \frac{d\alpha}{dz} + \alpha_f \rho_f u_f^2 \frac{du_f}{dz}$$

$$= \frac{6\alpha_m}{D_p} h_{tot}(T_m - T_{sat}) - 3/4\, c_D \rho_f u_f^3 \frac{\alpha_m}{D_p} - \alpha_f \rho_f u_f g \tag{A2.9}$$

The heat transfer models described in section 3.4 were again used in this model and the drag term was modelled using equation 12 with the drag coefficient given in equation 13.

Equation A2.2 was integrated to give the following relation

$$\alpha_f \rho_f u_f = u_f^{(o)} (1 - \alpha_m^{(o)}) \left(\alpha^{(o)} \rho_v + (1 - \alpha^{(o)}) \rho_l\right) \tag{A2.10}$$

Equations A2.5 and A2.9 were integrated numerically after equation A2.10 had been used to eliminate the fluid volume fraction. No problems were encountered with this integration and a Runge-Kutta method was found to give good results [28].

The initial conditions were of a similar form to those described for the previous model. A fixed melt volume fraction was specified at the falling melt front and the vapour volume fraction was set to zero in most of the calculations, since these conditions were used by Bankoff and Han. It was decided to either prescribe an arbitrary value for the fluid velocity (corresponding to ISTART=0) or to use the terminal velocity (ISTART=1).

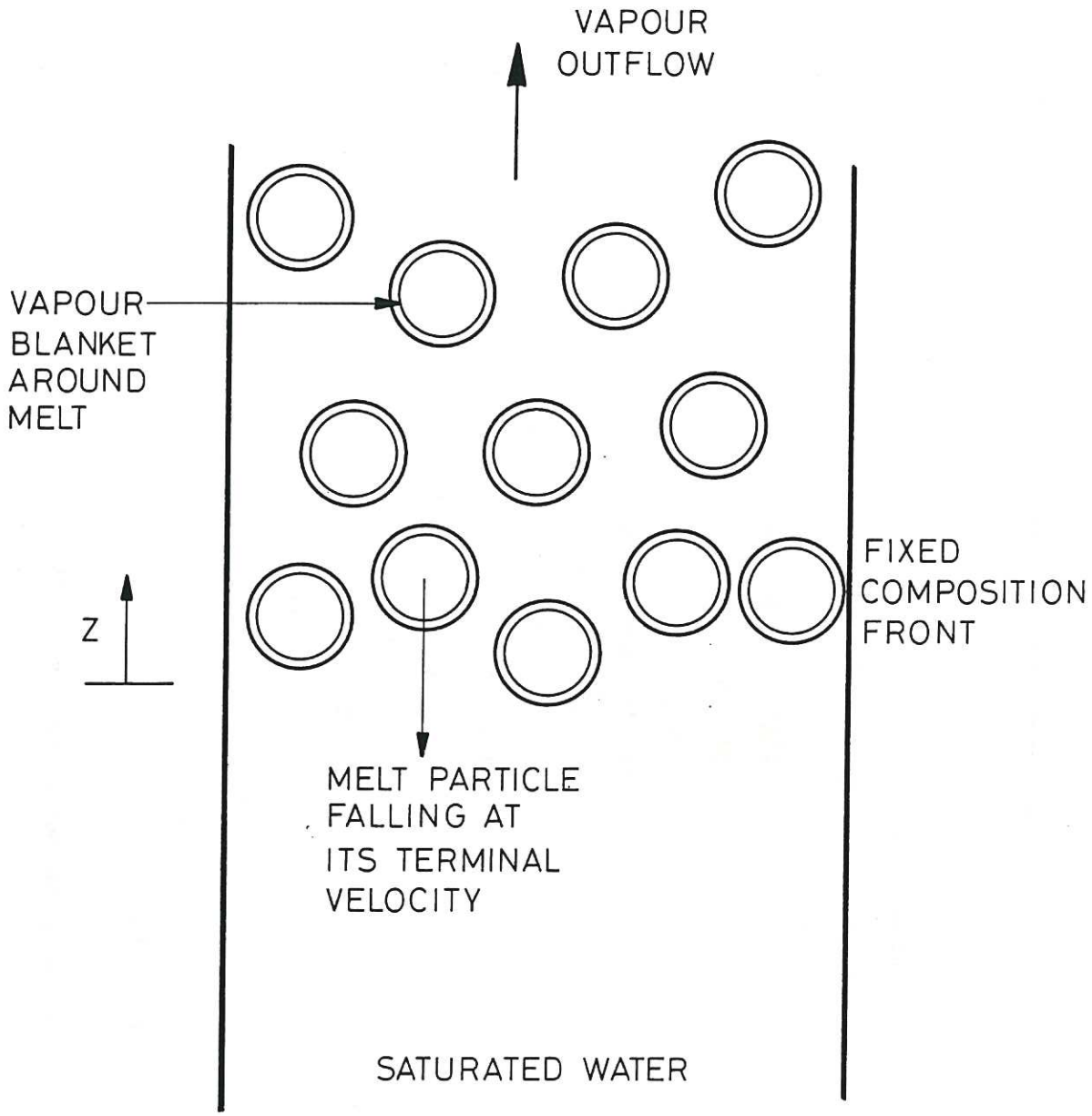

Fig. 1 A schematic representation of the 1D steady state model of Bankoff and Han.

CLM-R252

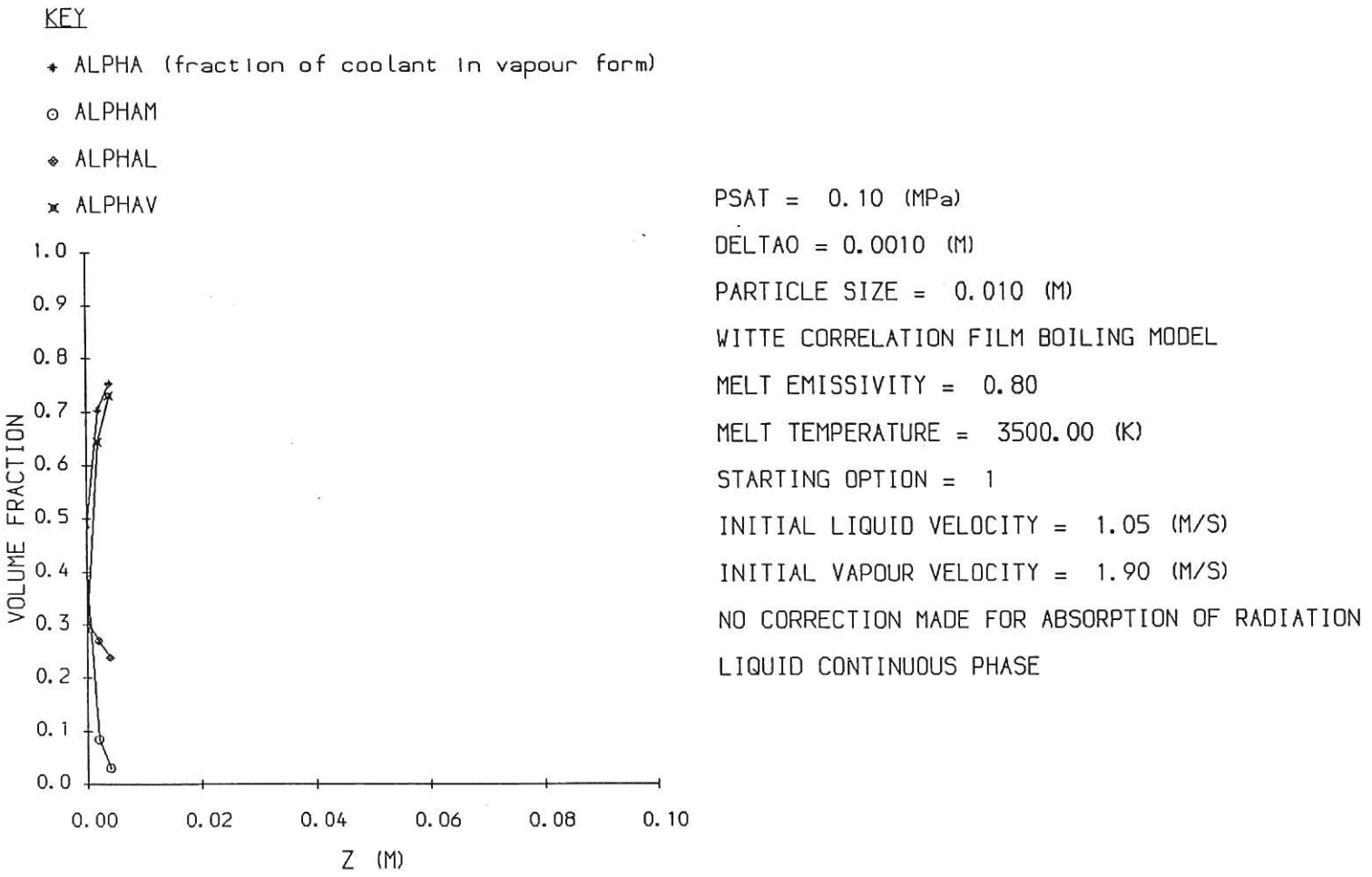

Fig. 2 Volume fraction results for a pressure of 0.1 MPa.

CLM-R252

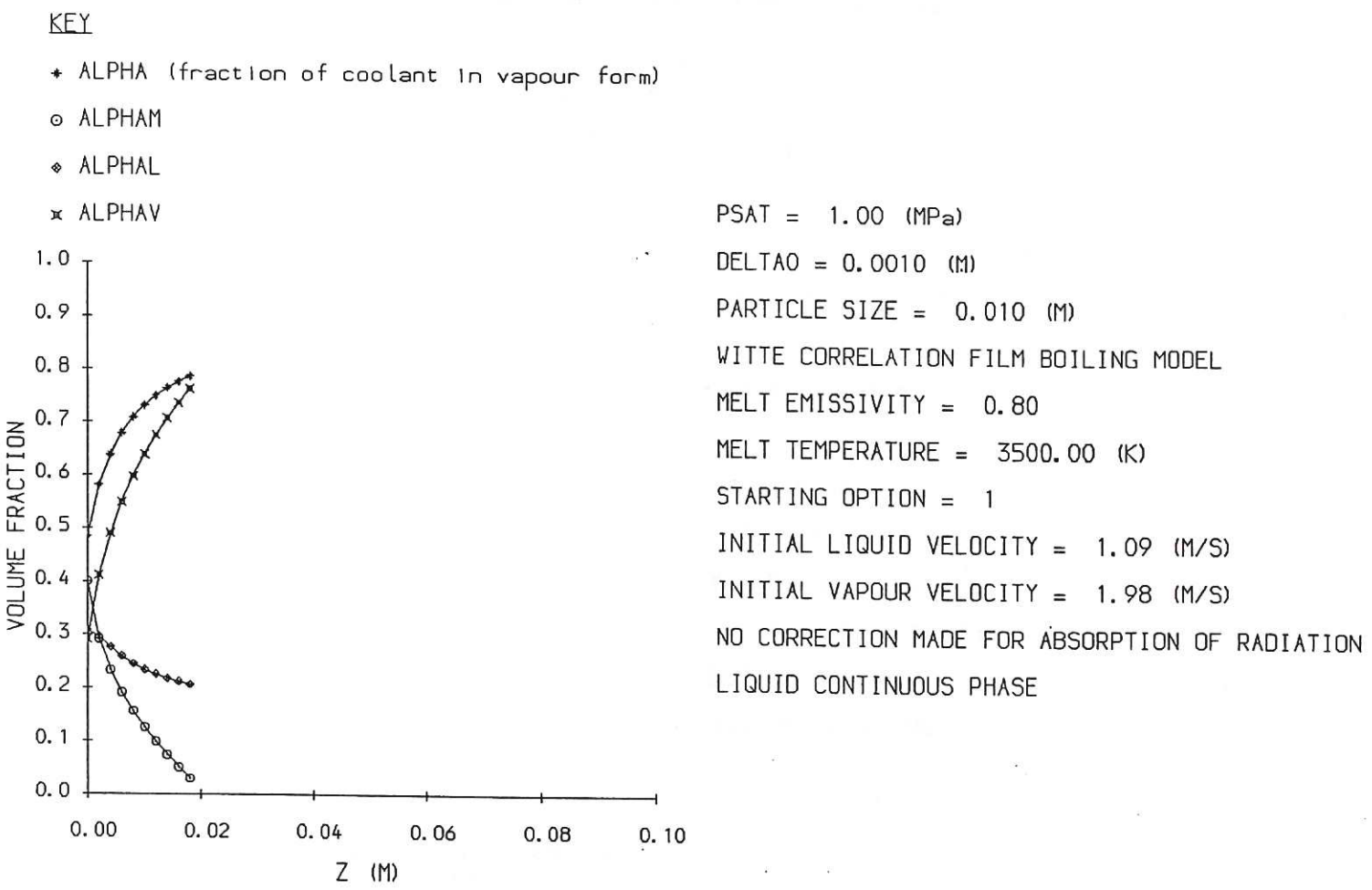

Fig. 3 Volume fraction results for a pressure of 1.0MPa.

CLM-R252

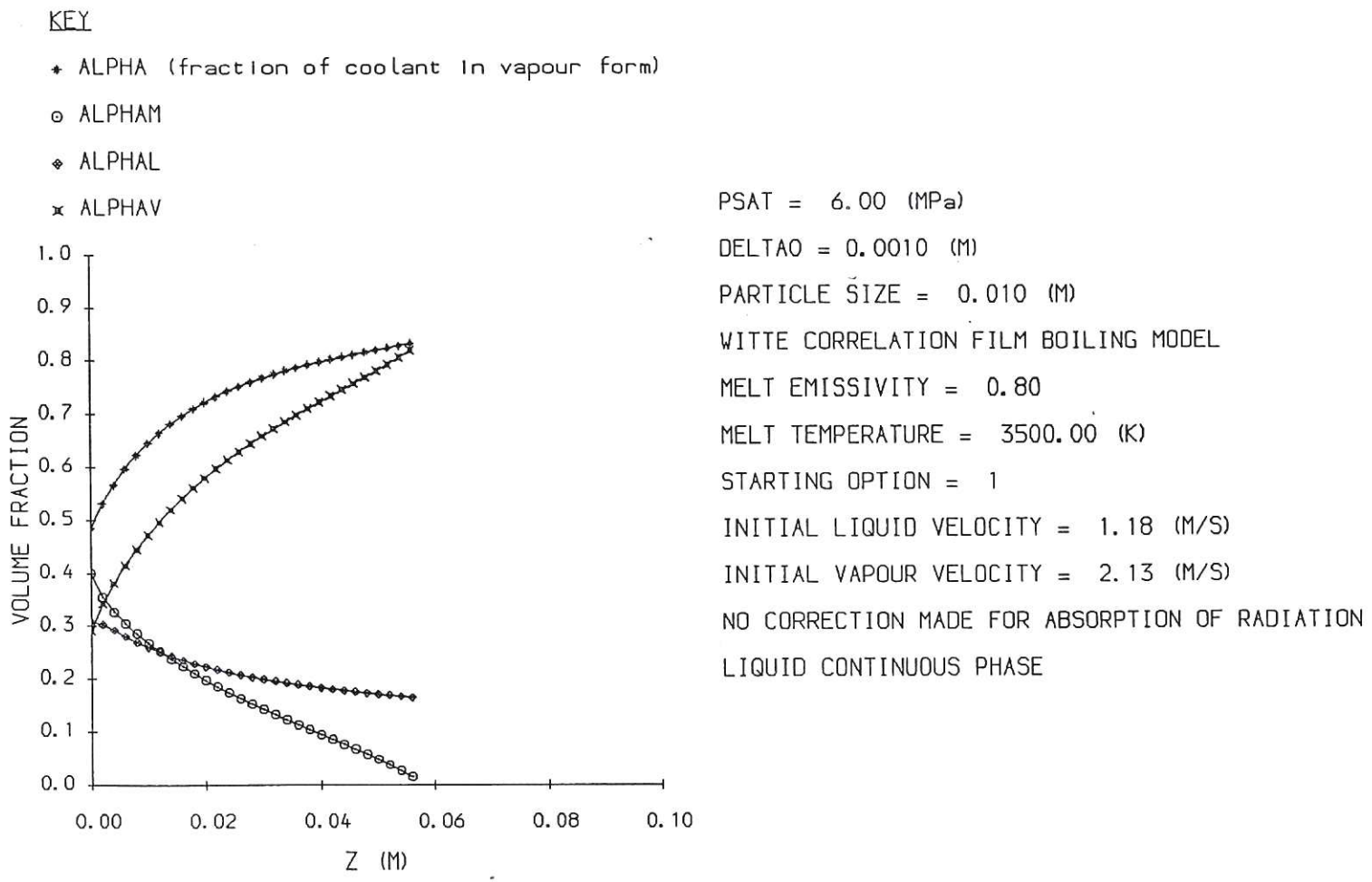

Fig. 4 Volume fraction results for a pressure of 6.0MPa.

CLM-R252

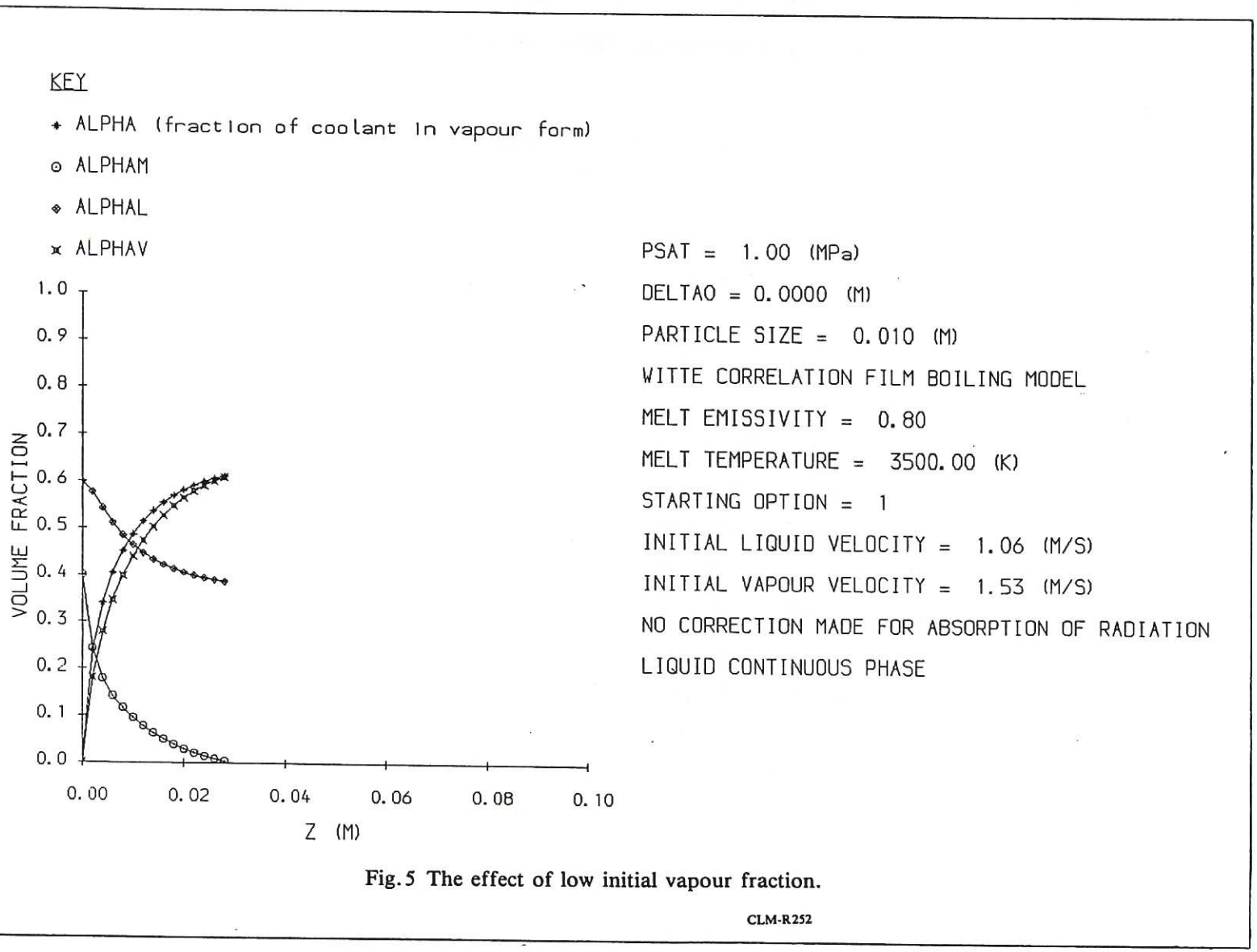

Fig. 5 The effect of low initial vapour fraction.

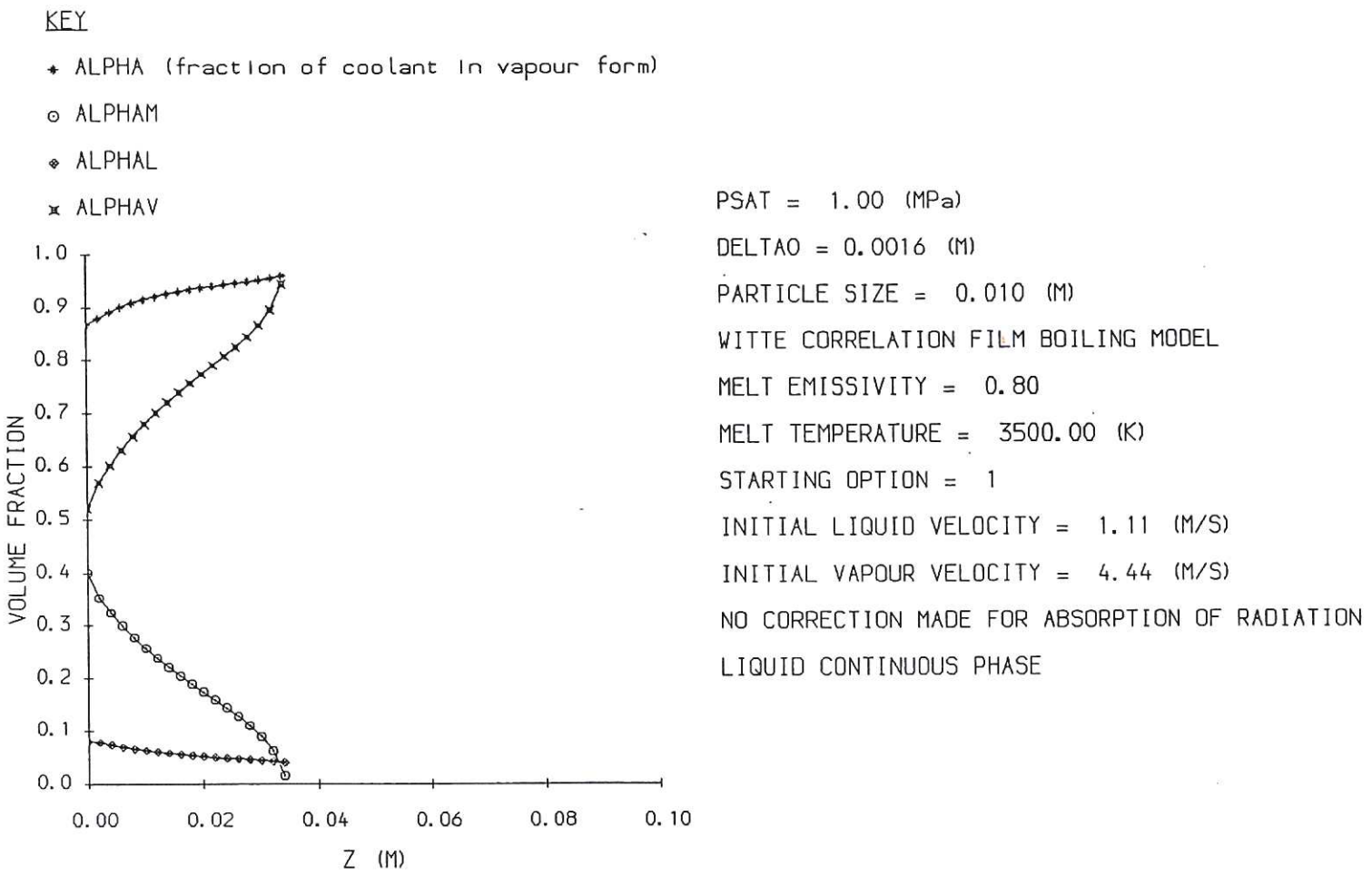

Fig.6 Results for a vapour film thickness of 1.6mm.

CLM-R252

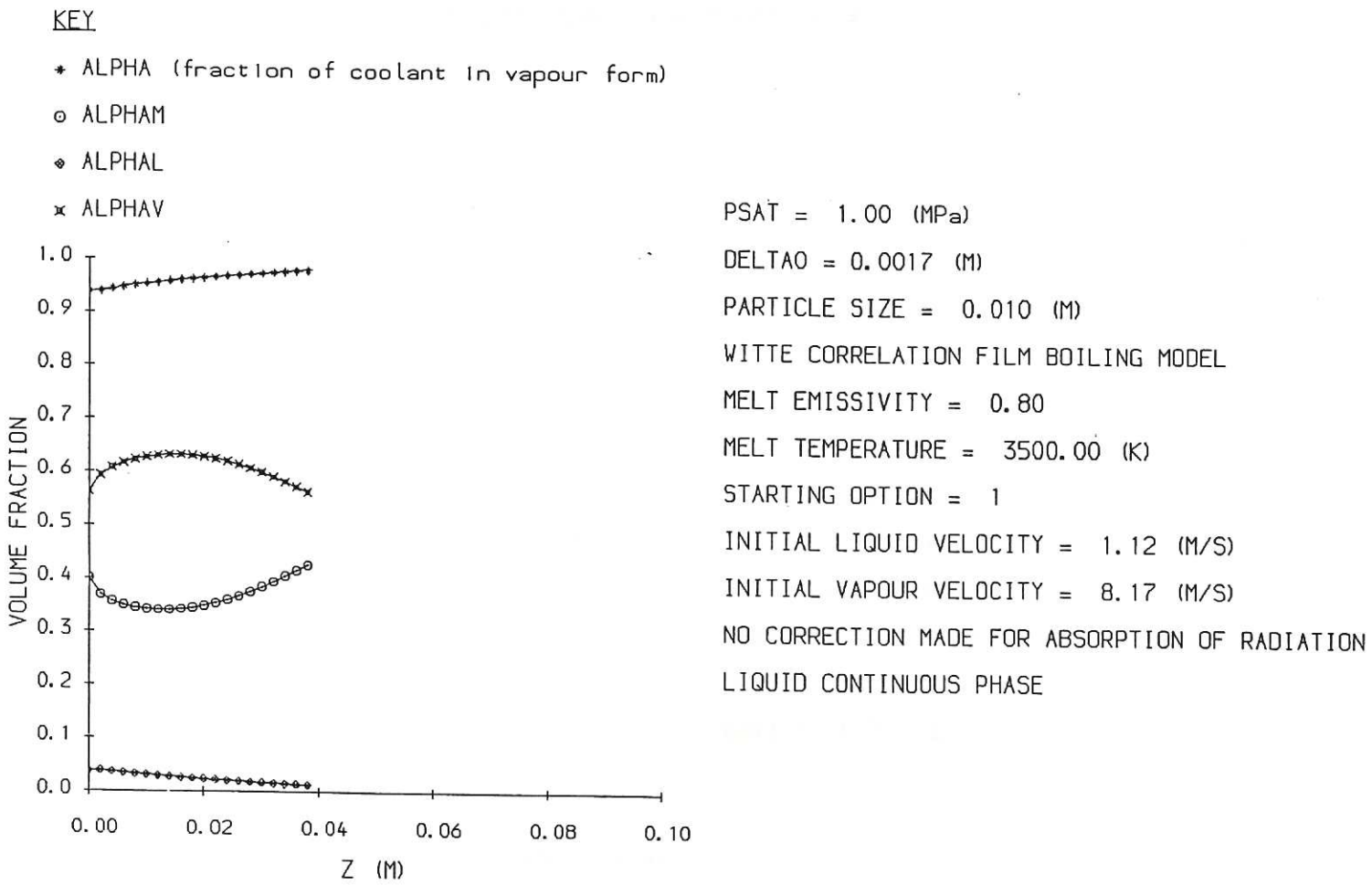

Fig.7 Results for a vapour film thickness of 1.7mm.

CLM-R252

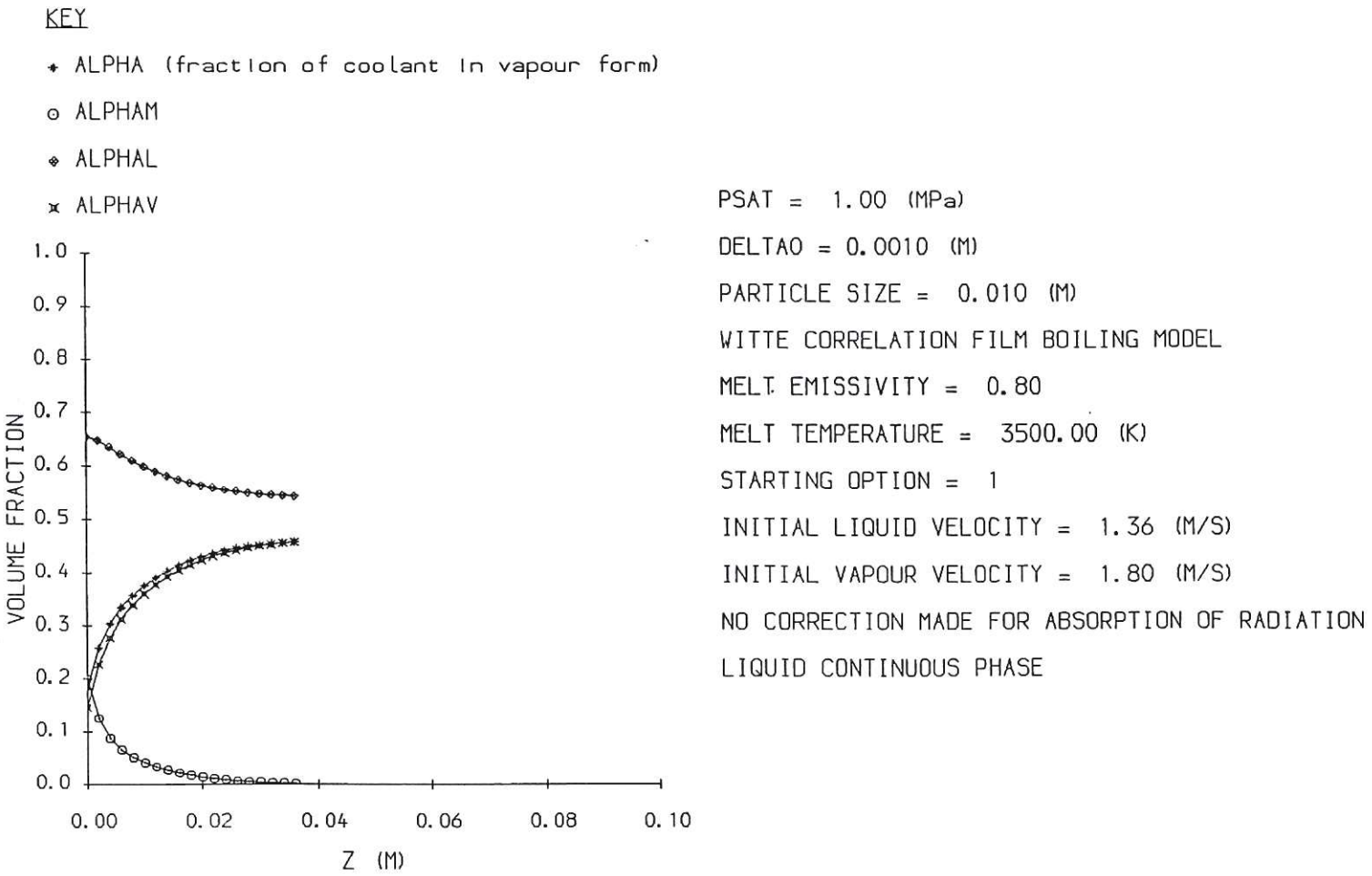

Fig. 8 The effect of low initial melt fraction.

CLM-R252

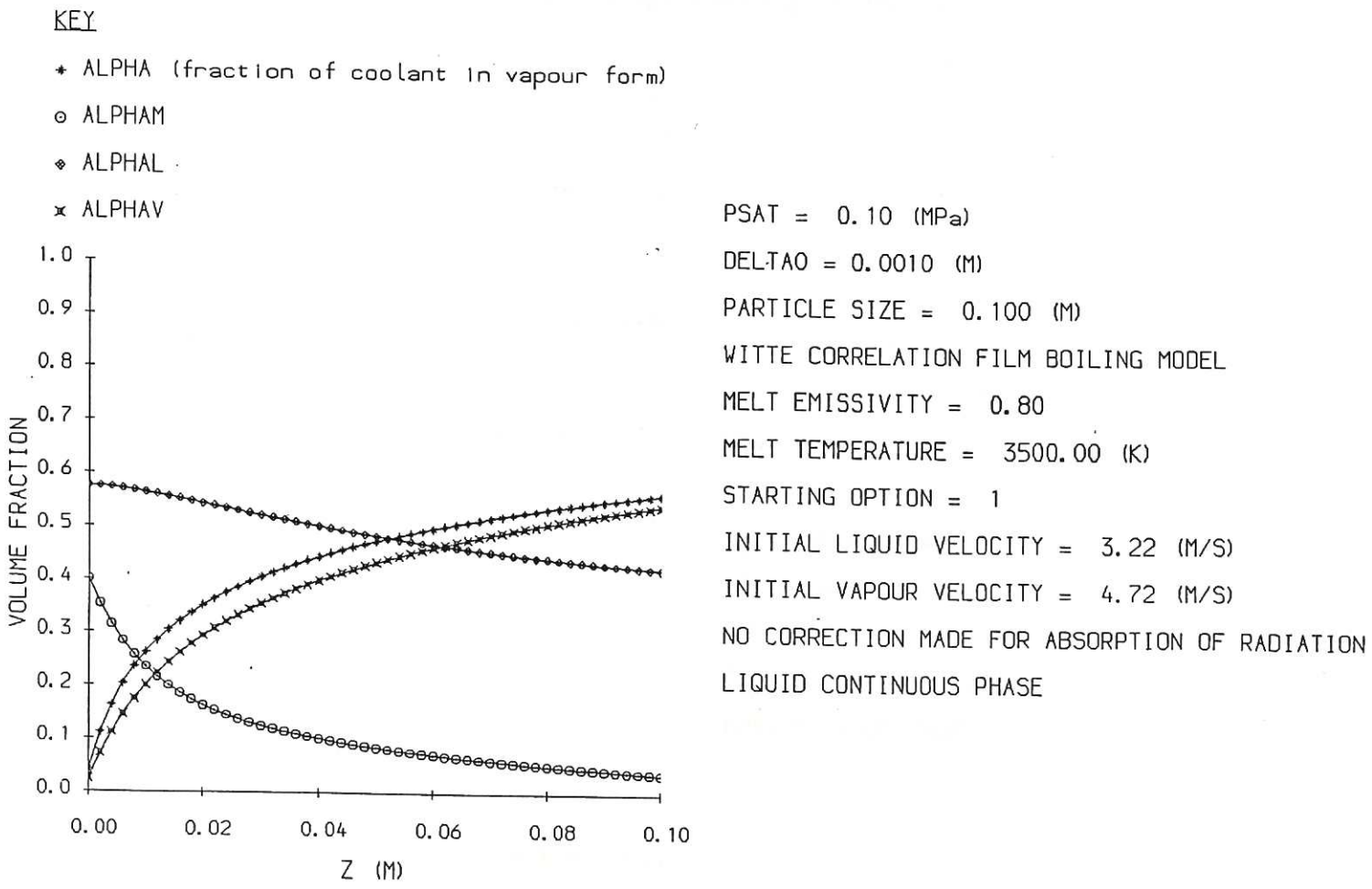

Fig. 9 The effect of increased particle size (at 0.1 MPa).

CLM-R252

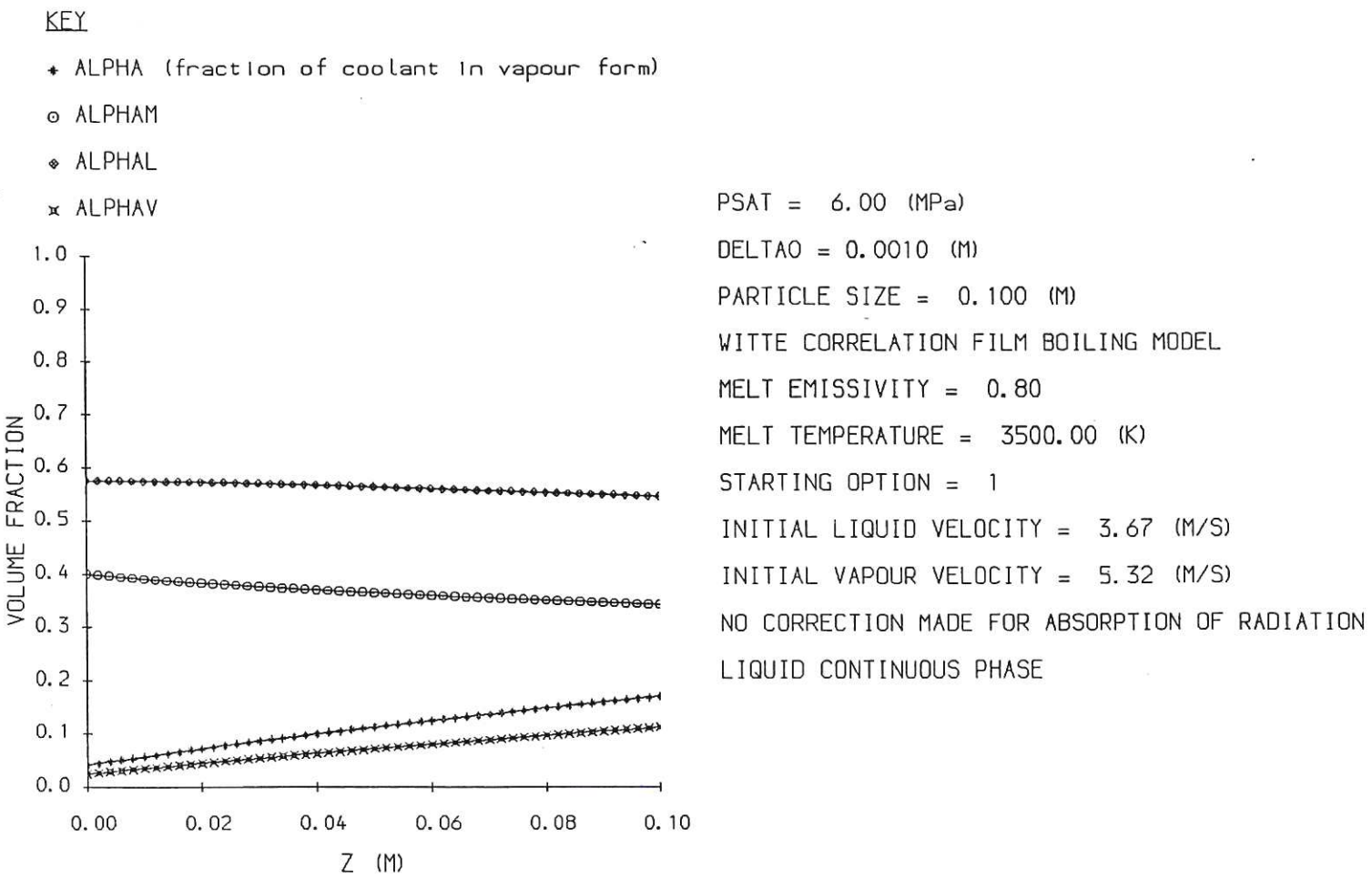

Fig. 10 The effect of increased particle size (at 6.0MPa).

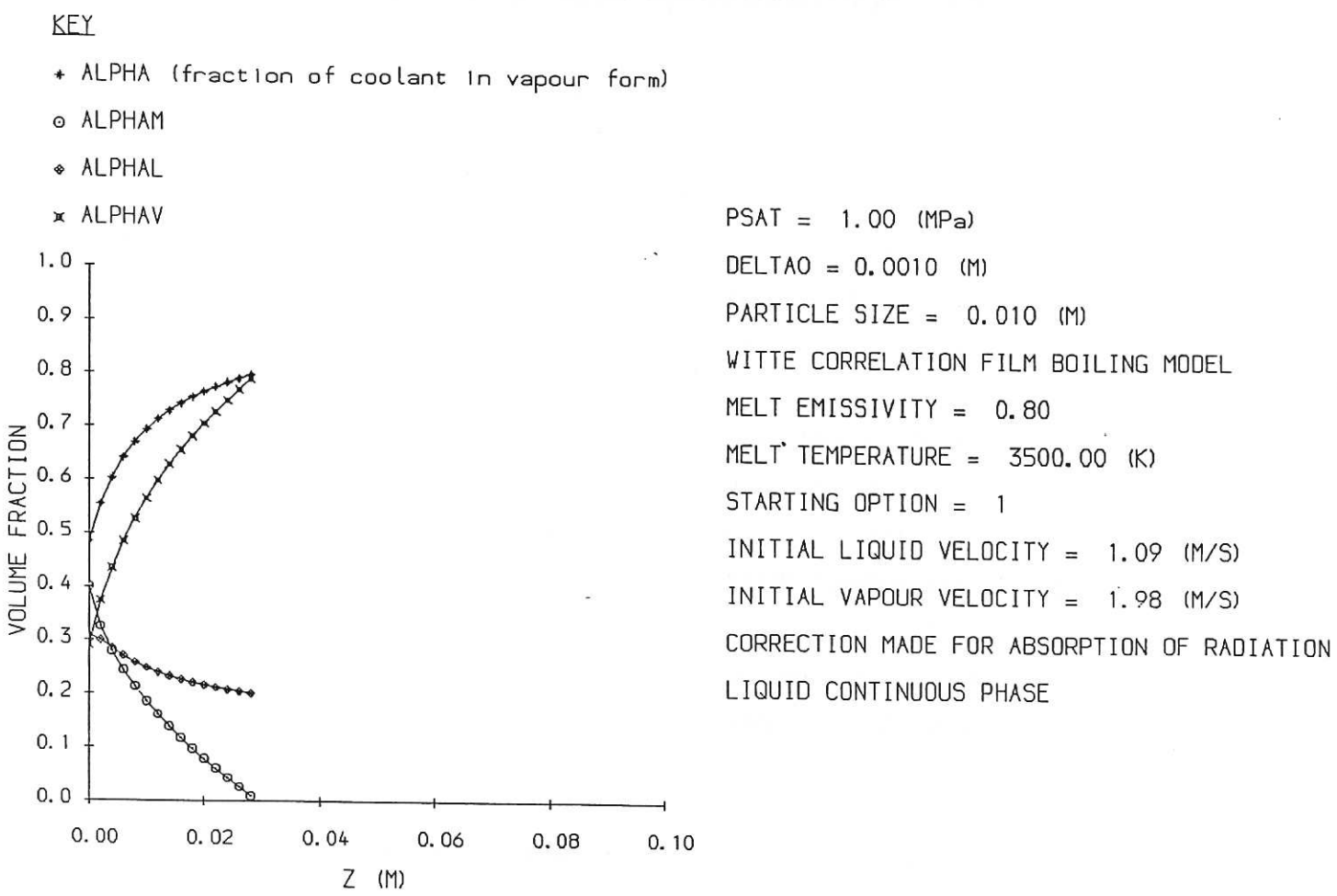

Fig. 11 Results for a modified radiation model (high liquid fraction).

CLM-R252

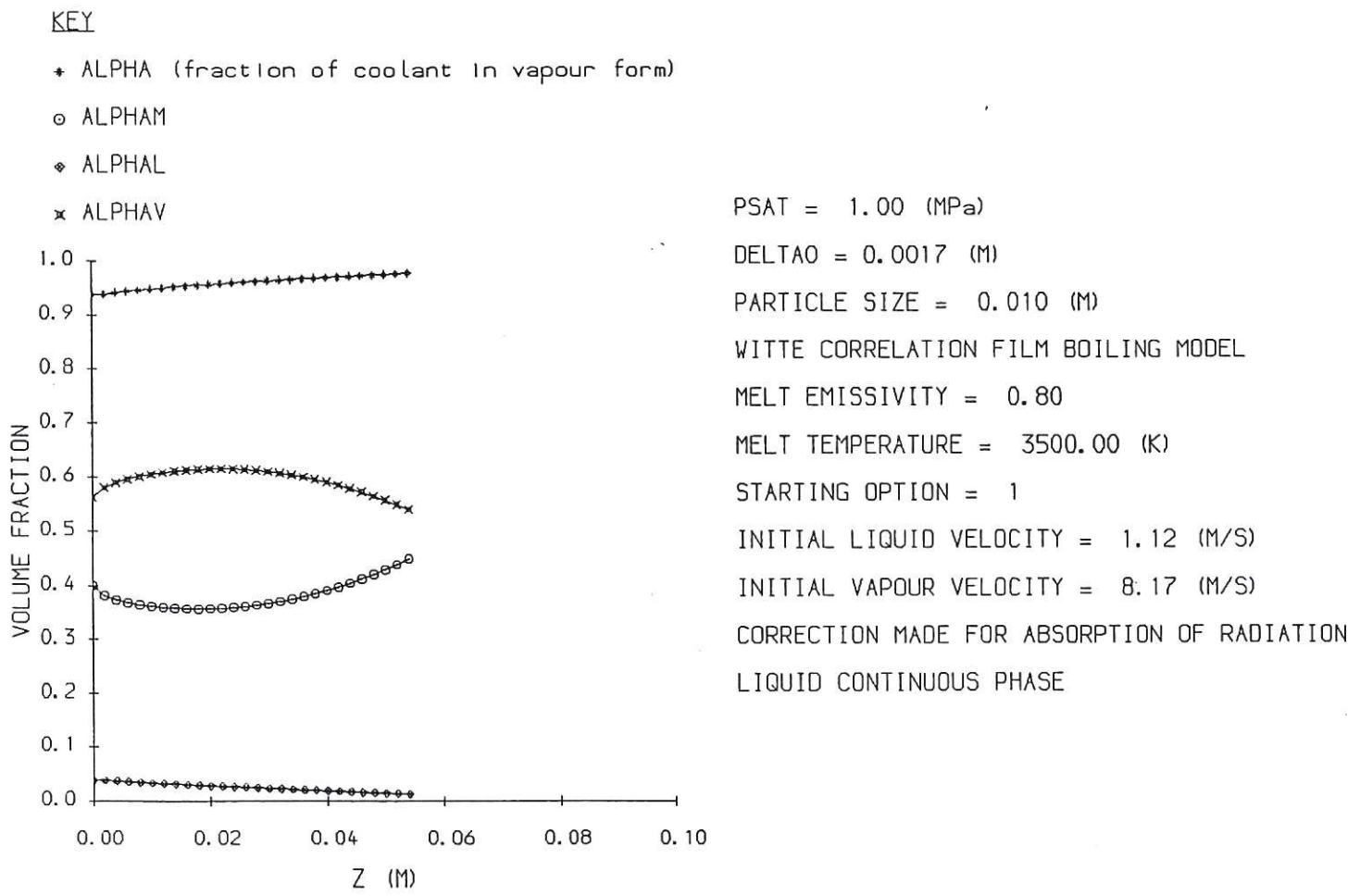

Fig. 12 Results for a modified radiation model (low liquid fraction).

CLM-R252

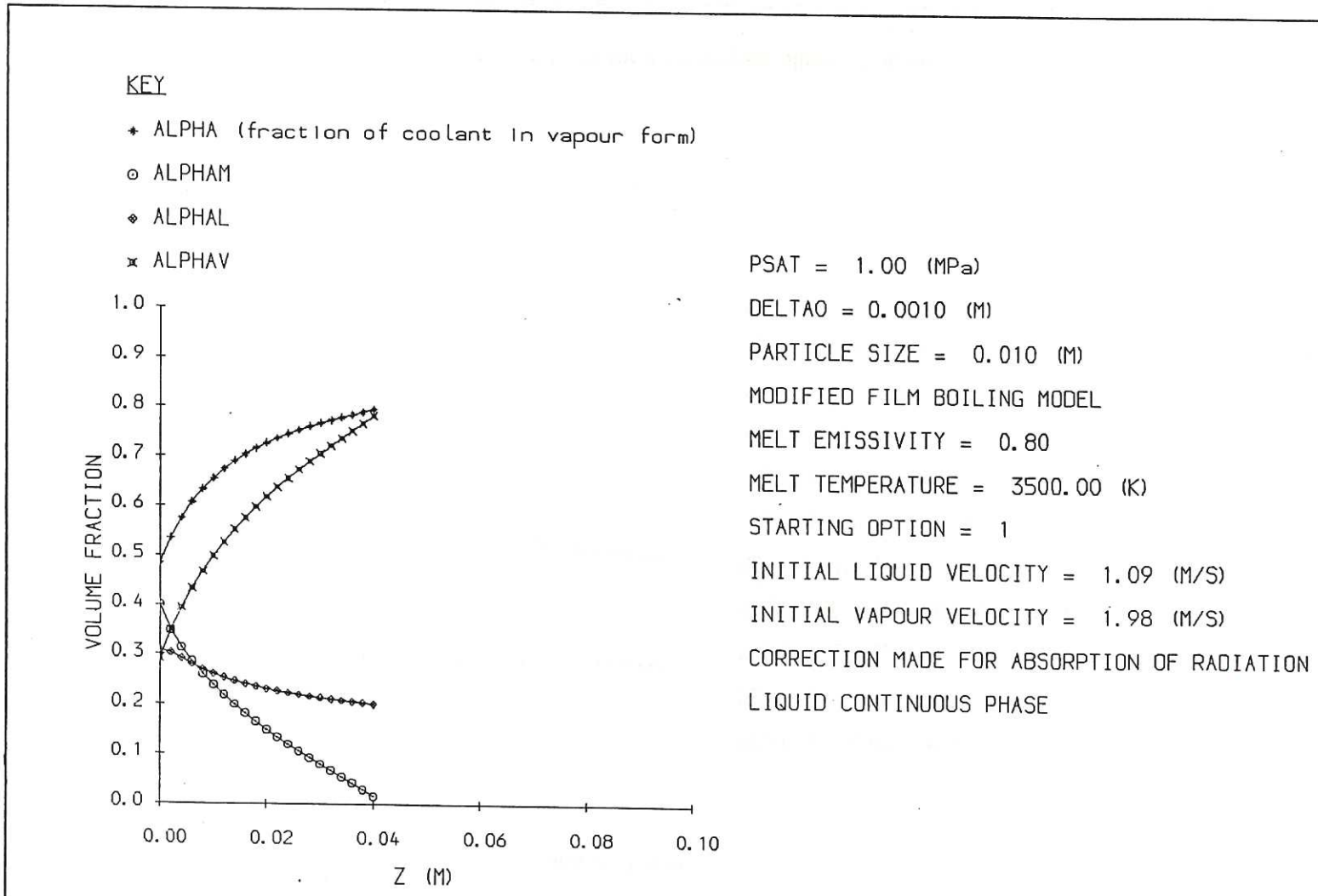

Fig. 13 Results using a modified boiling model.

CLM-R252

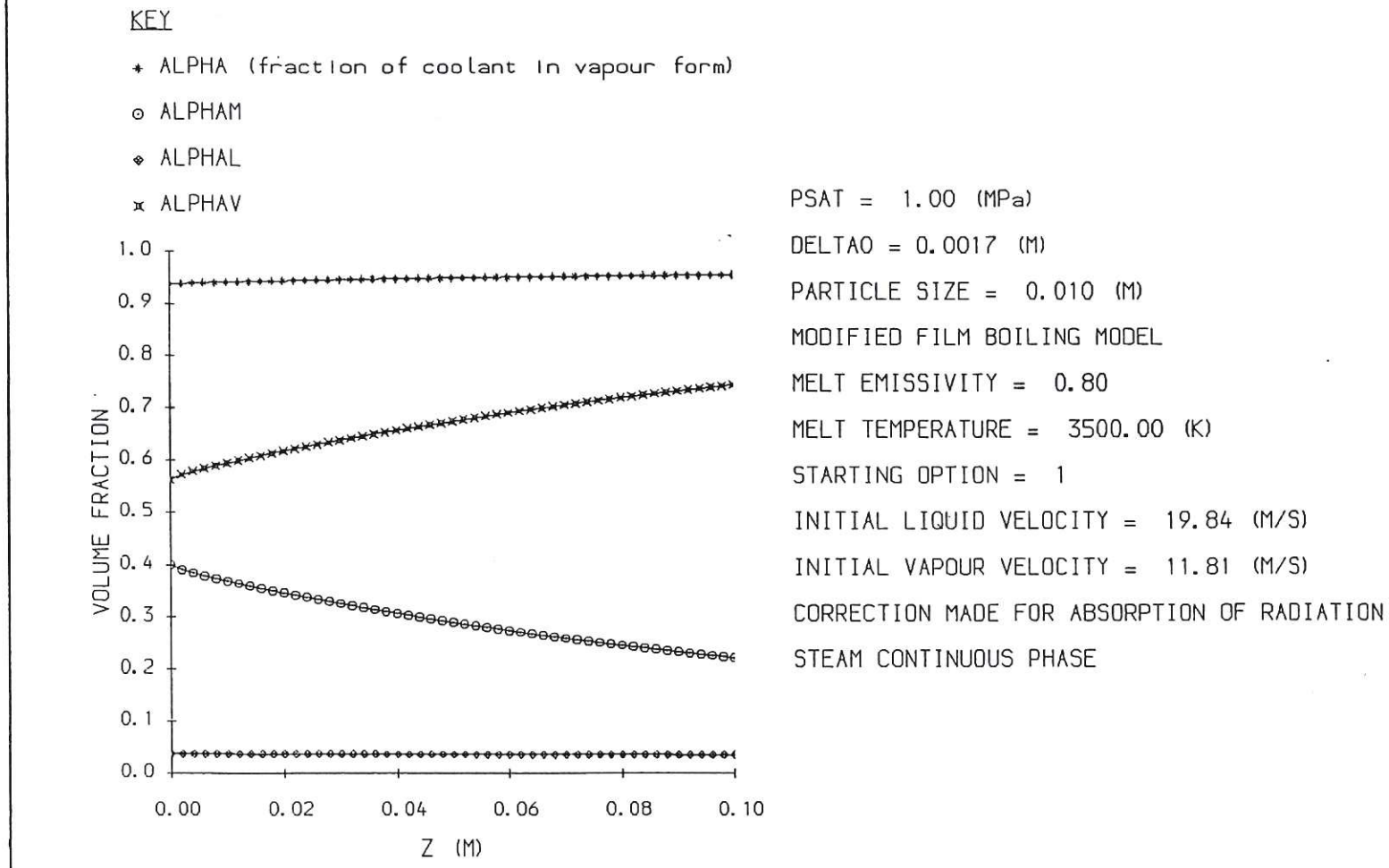

Fig. 14 Results for a continuous phase of vapour.

CLM-R252

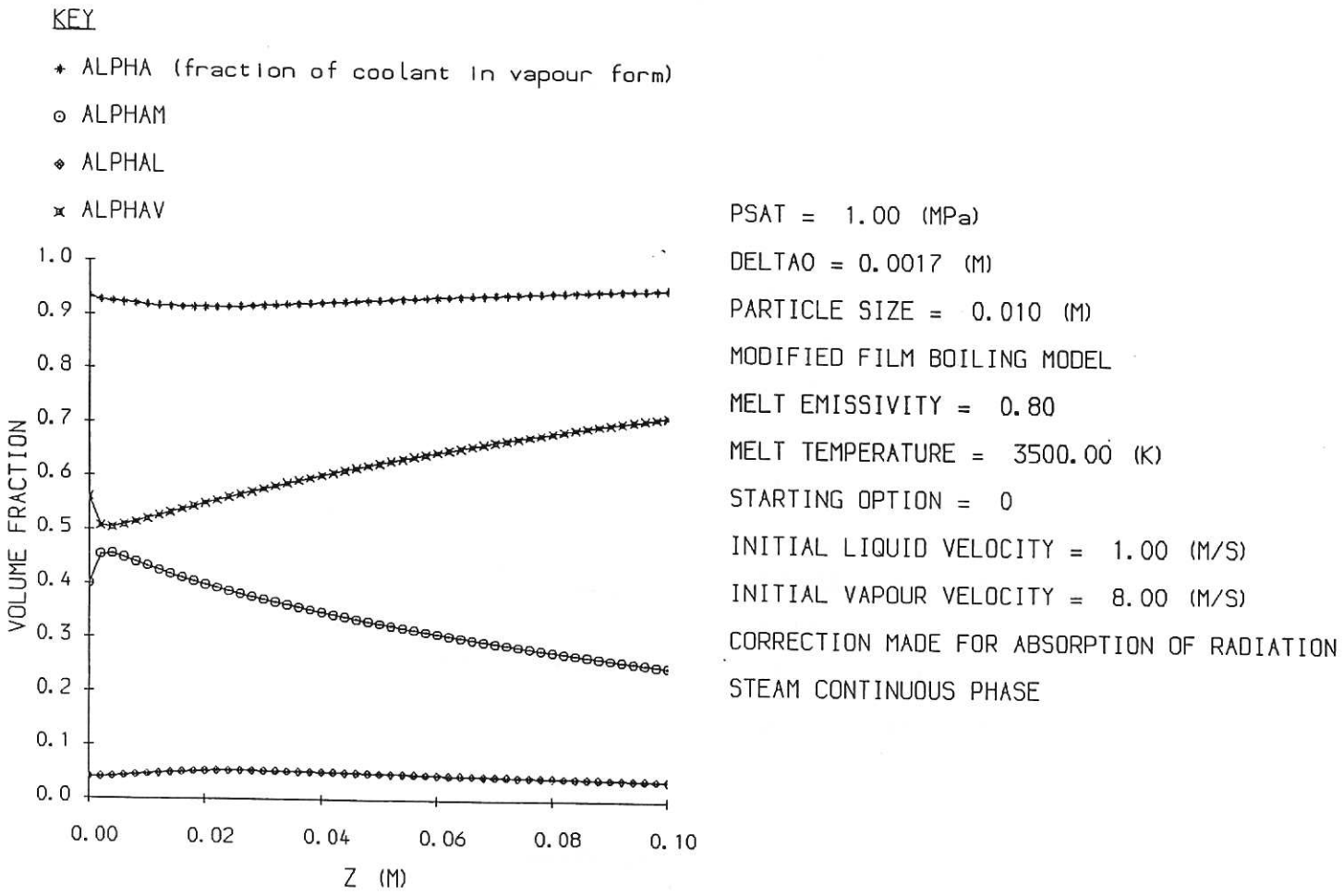

Fig. 15 Results for a continuous phase of vapour above the melt front.

CLM-R252

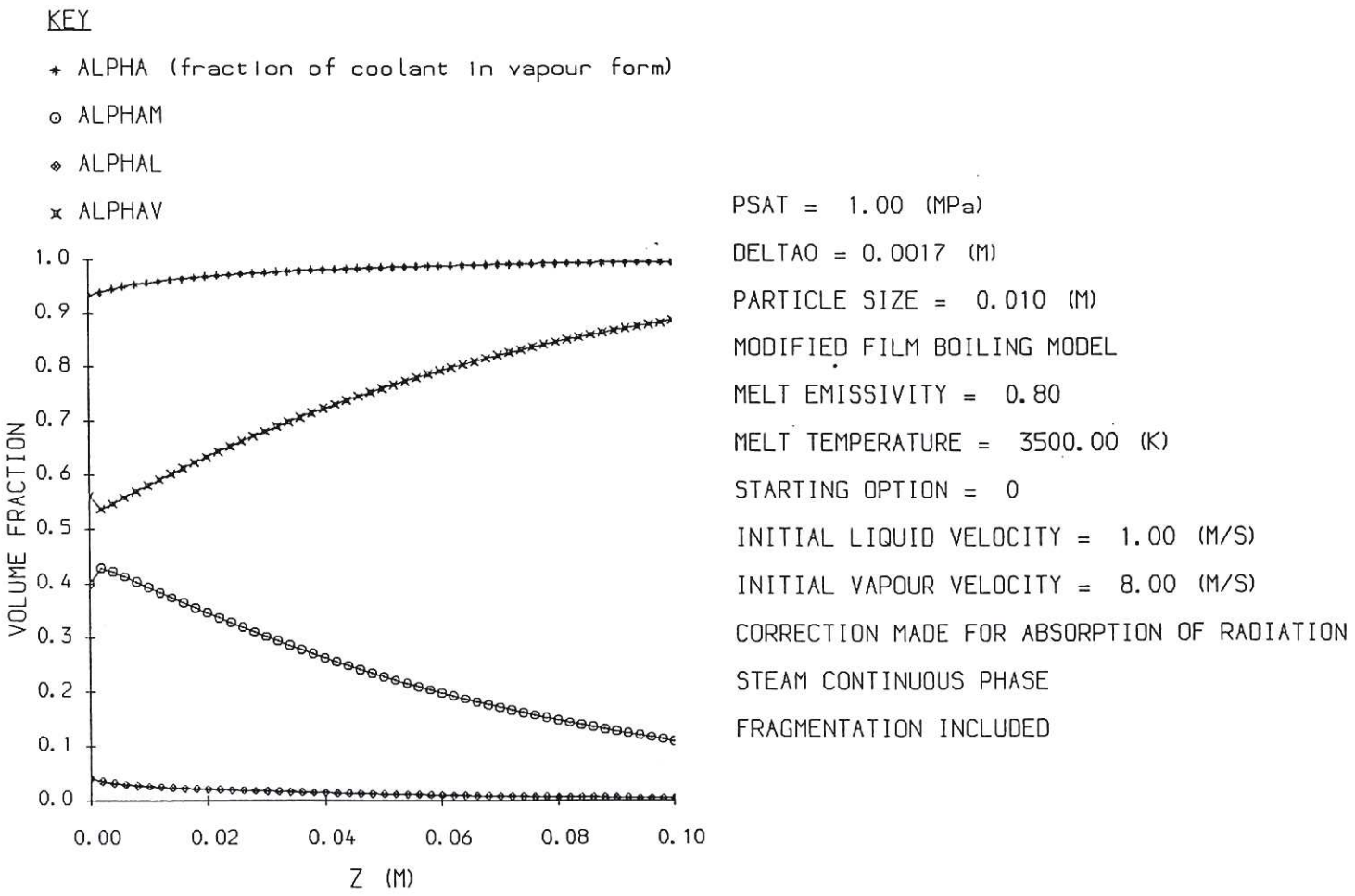

Fig16 Results using a simple break-up model.

CLM-R252

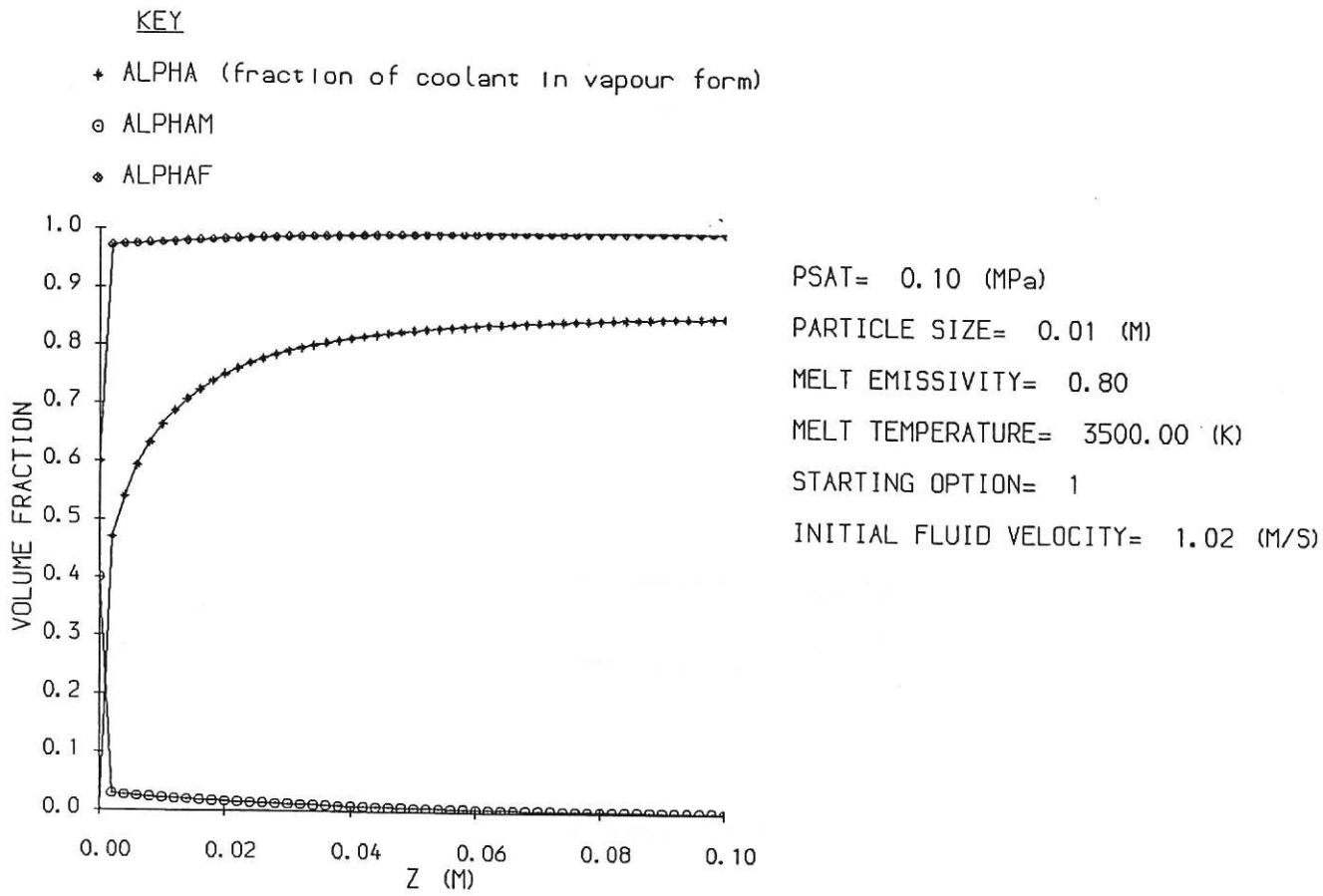

Fig. 17 Homogeneous flow results for a pressure of 0.1 MPa.

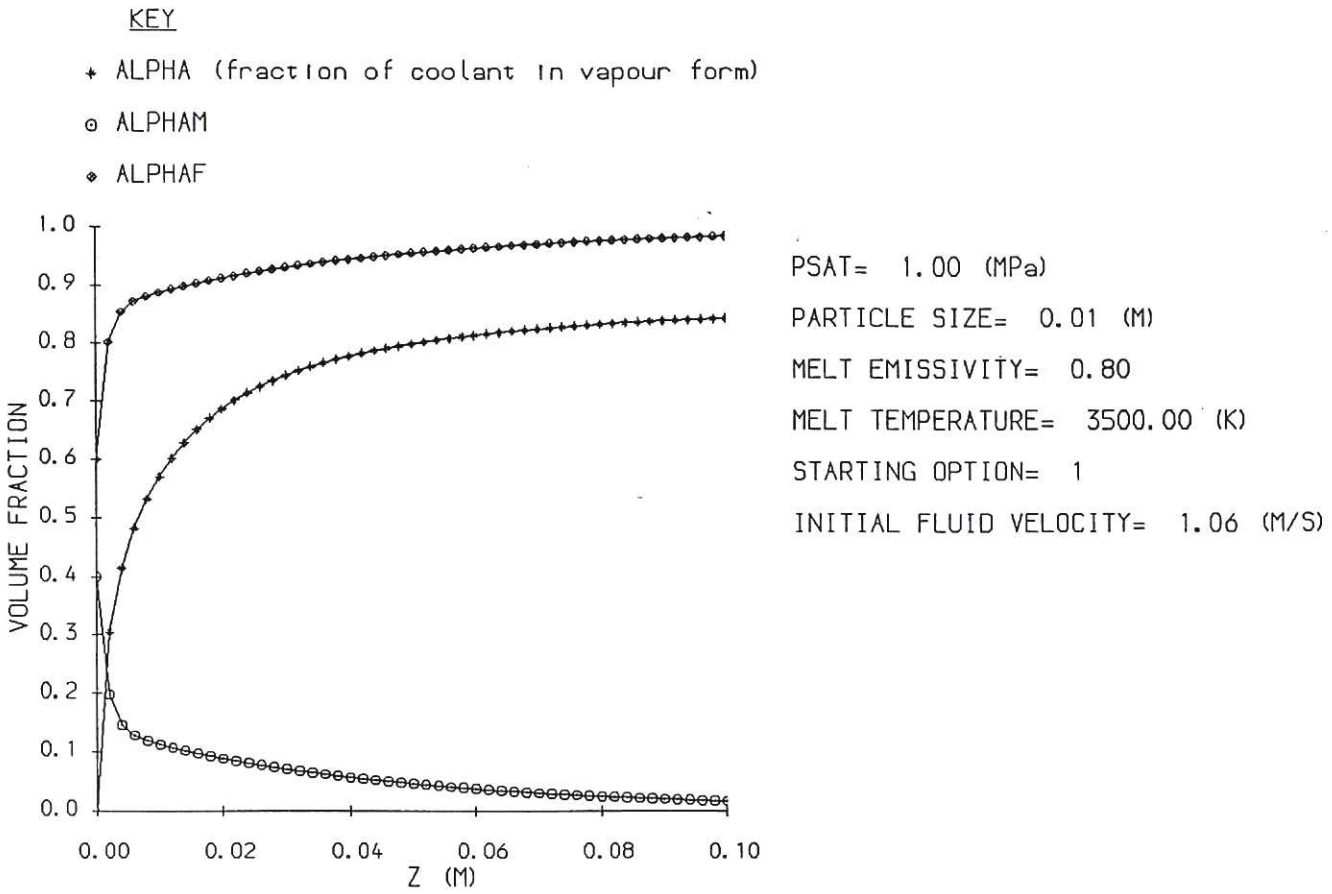

Fig. 18 Homogeneous flow results for a pressure of 1.0MPa.

CLM-R252

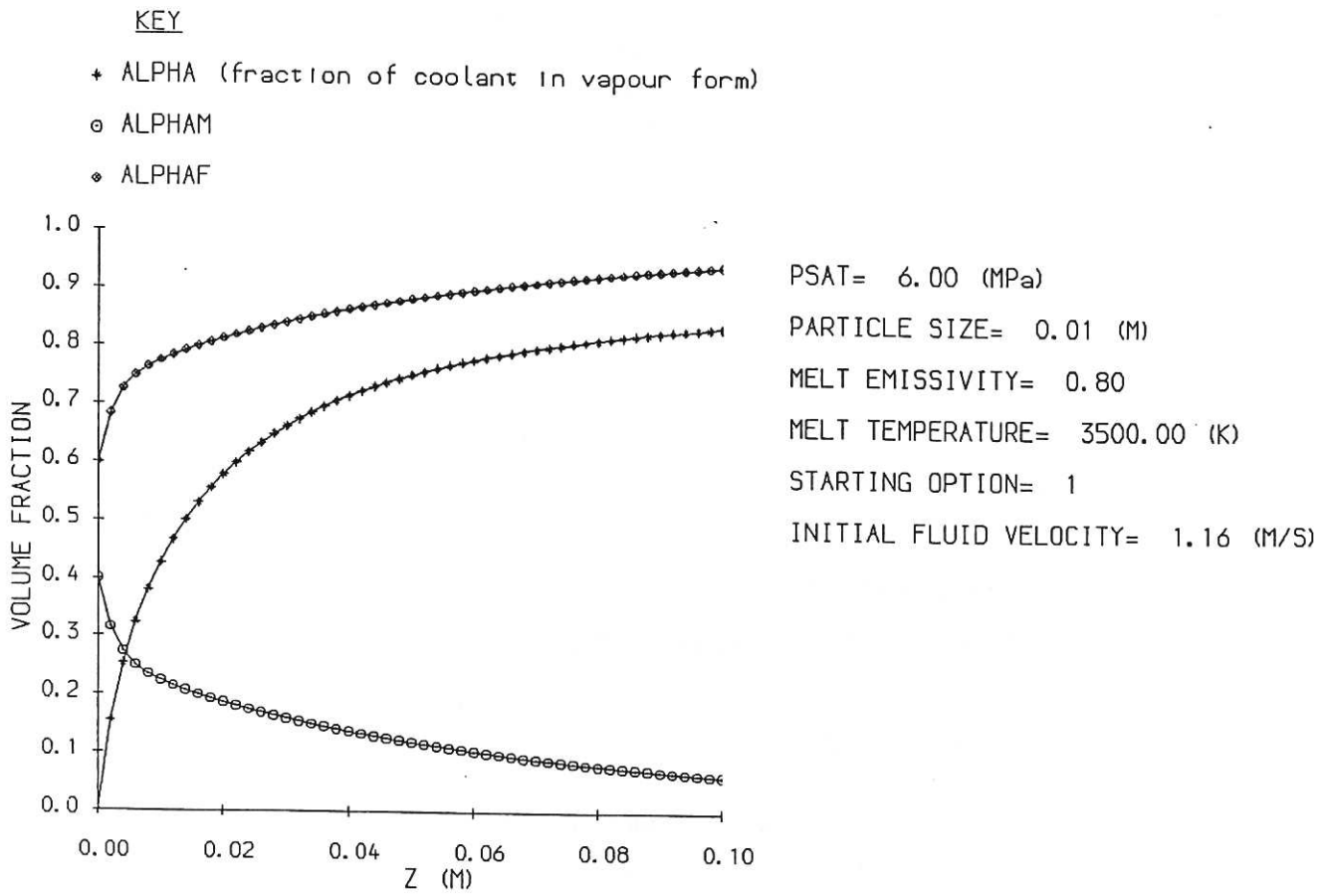

Fig. 19 Homogeneous flow results for a pressure of 6. 0MPa.

CLM-R252

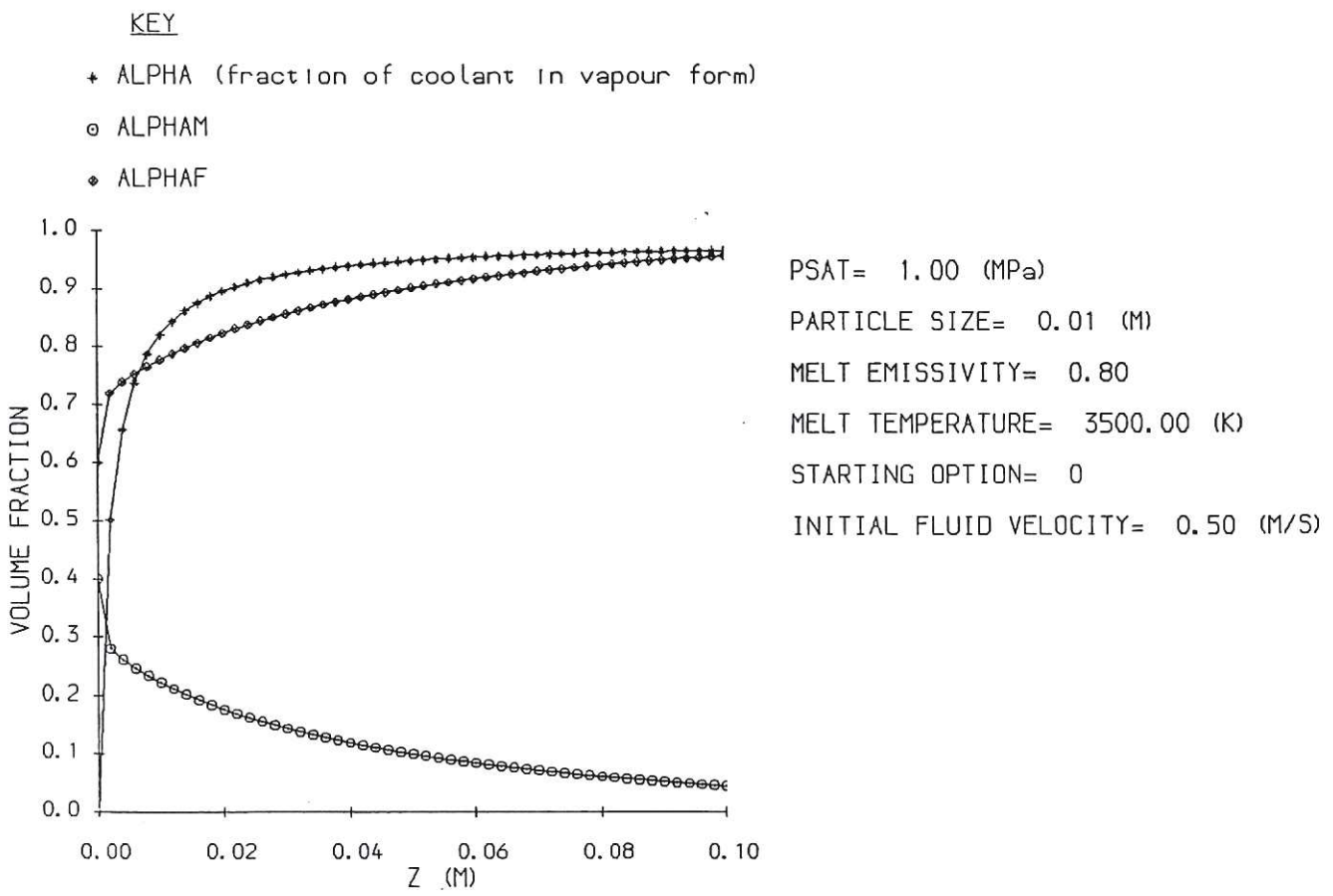

Fig. 20 Results for a pressure of 1MPa and an initial velocity of 0.5m/s.

CLM-R252

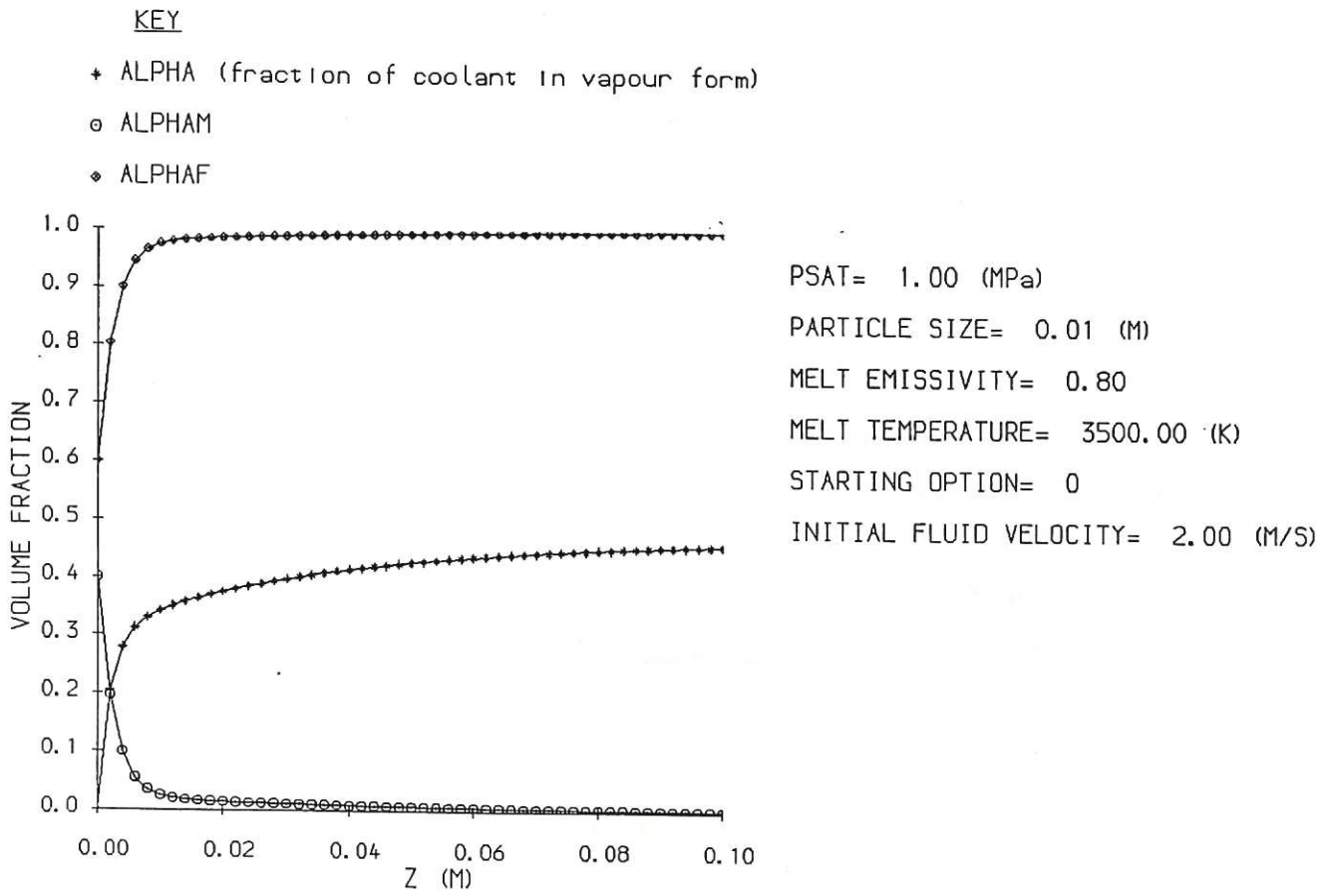

Fig. 21 Results for a pressure of 1MPa and an initial velocity of 2.0m/s.

CLM-R252

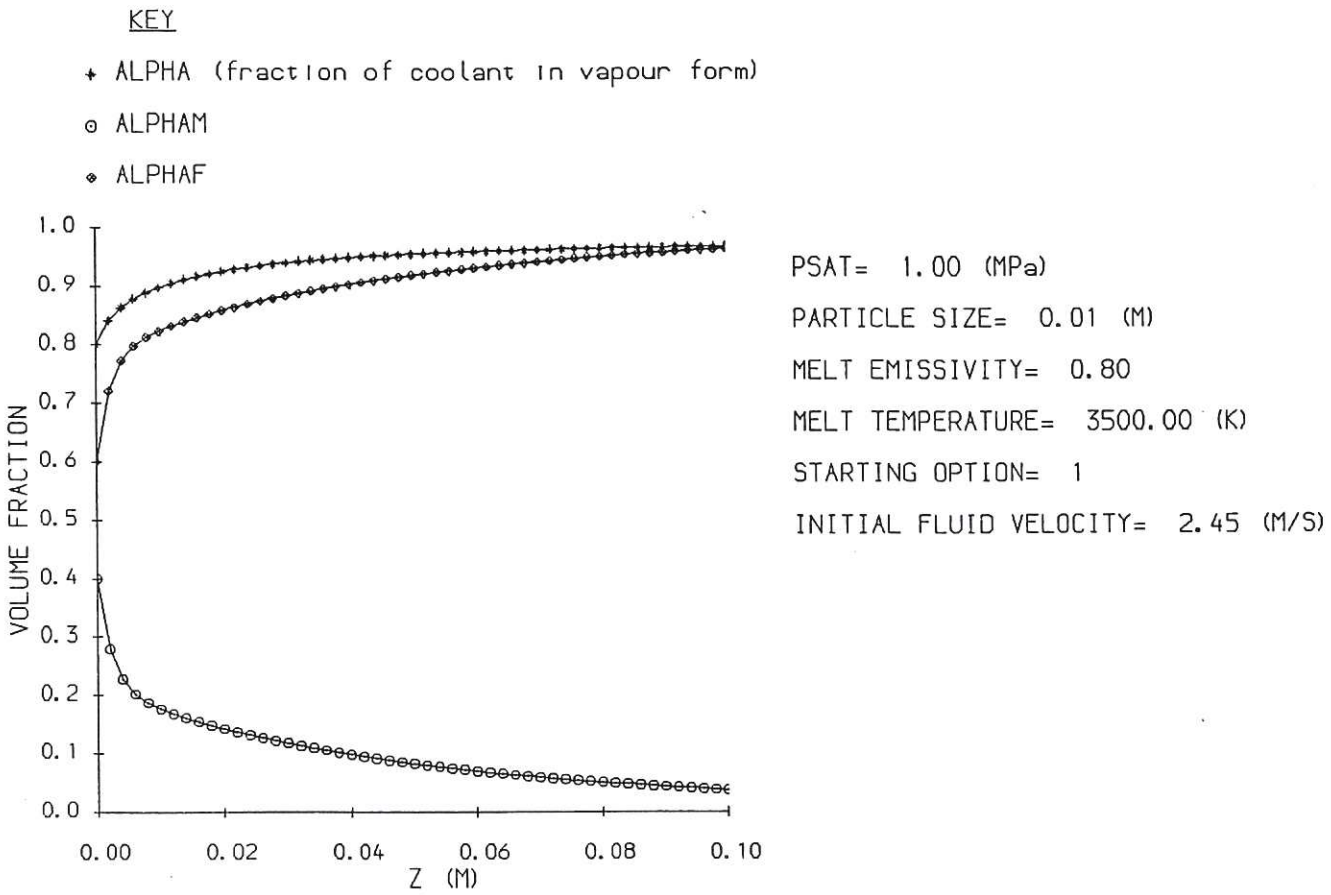

Fig. 22 Results for a pressure of 1MPa and an initial void fraction of 0.8.

CLM-R252

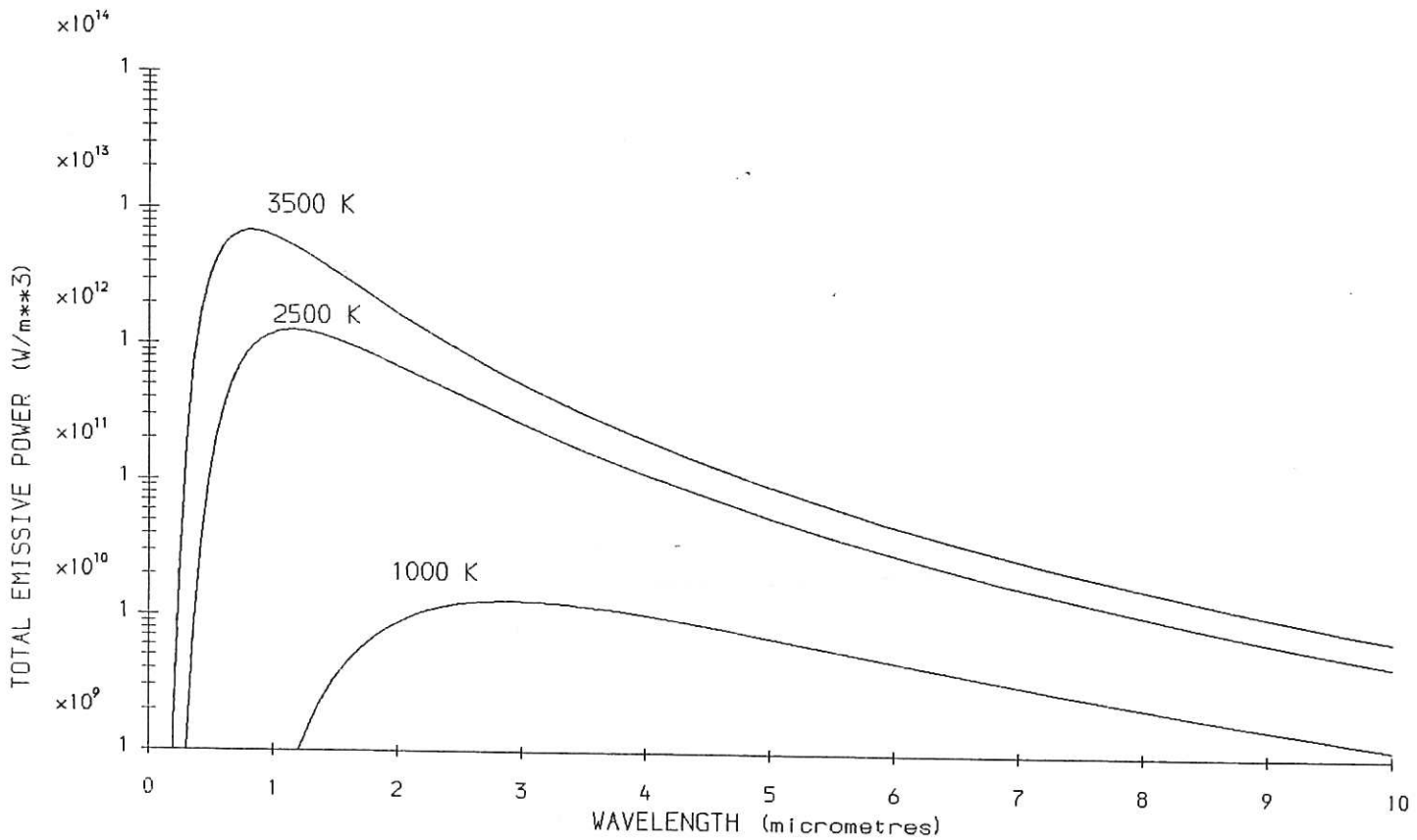

Fig. A1 The power spectrum for a blackbody radiation to a vacuum.

CLM-R252

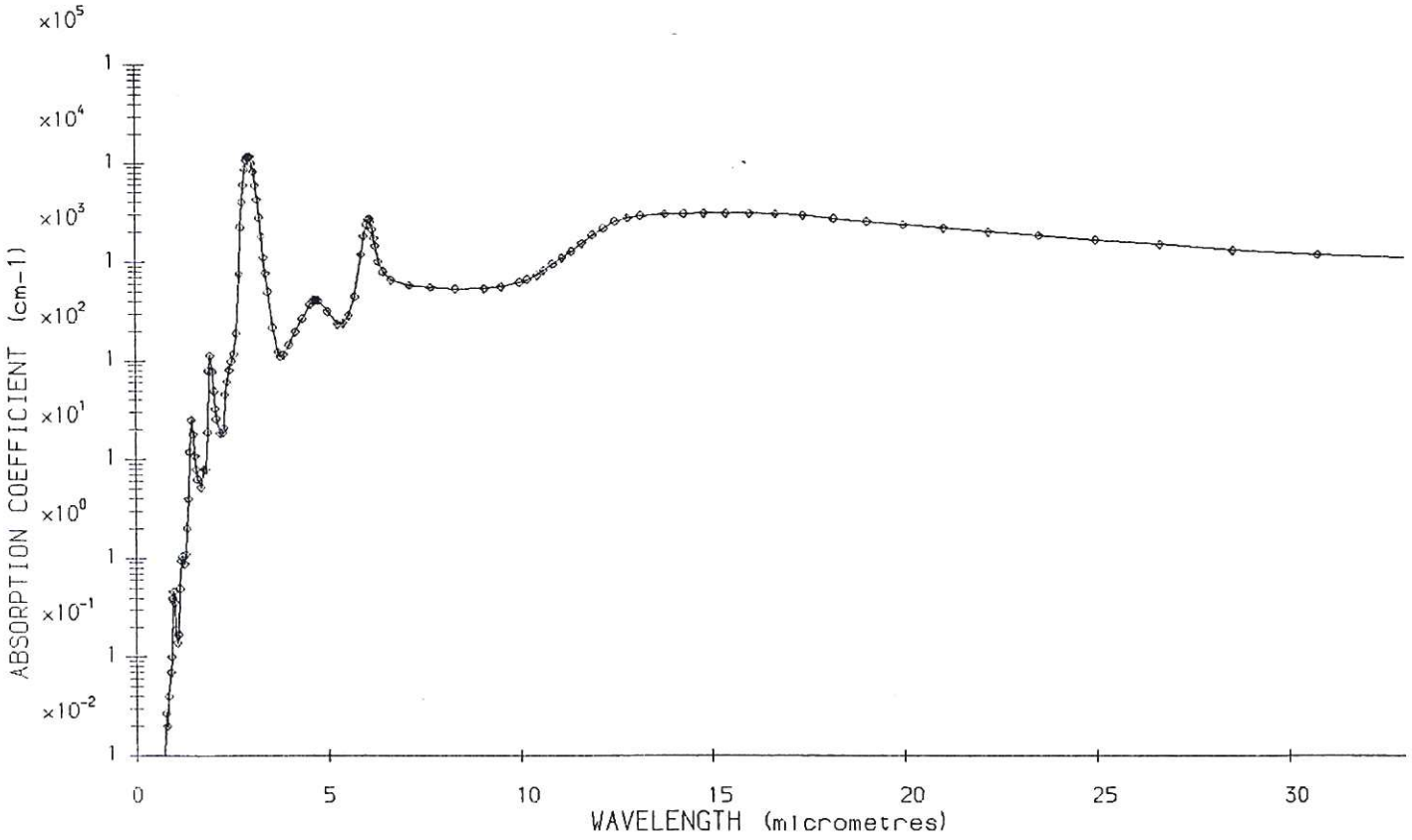

Fig. A2 The absorption coefficient of water at 20°C and 1 Bar.

CLM-R252

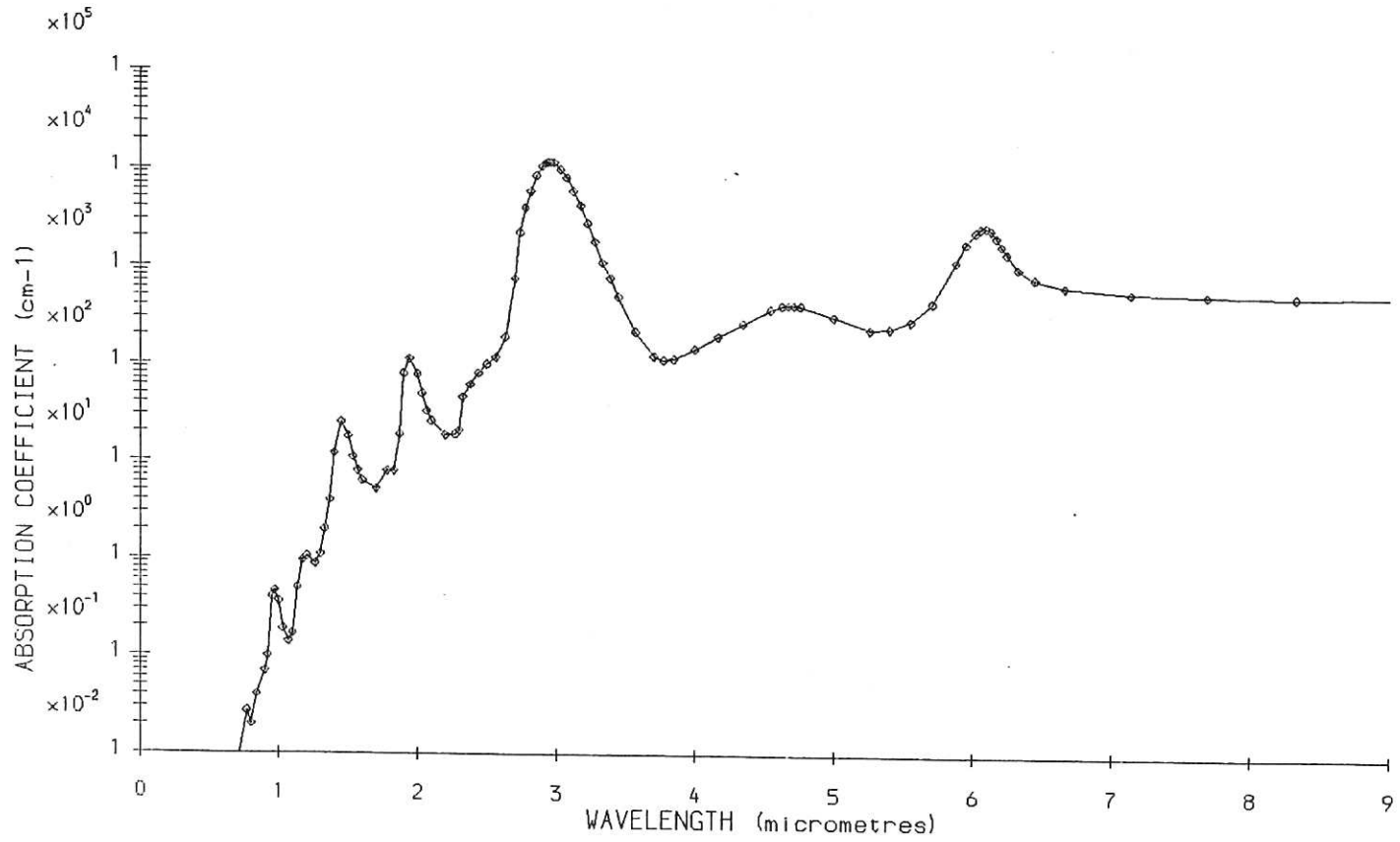

Fig. A3 The absorption coefficient of water at 20° C and 1 Bar (detailed view of absorption banos).

CLM-R252

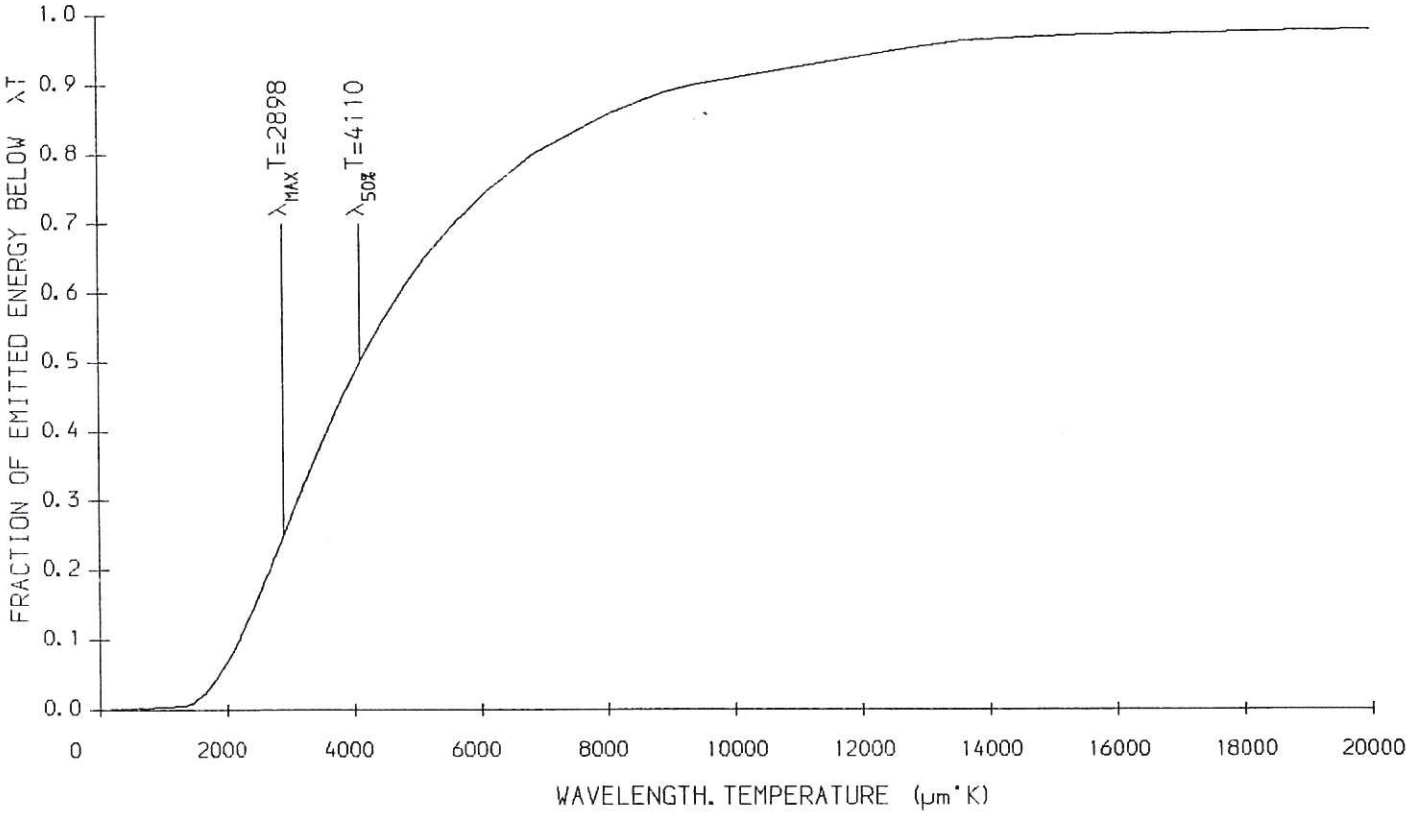

Fig. A4 The distribution of emissive power as a function at λT.

CLM-R252

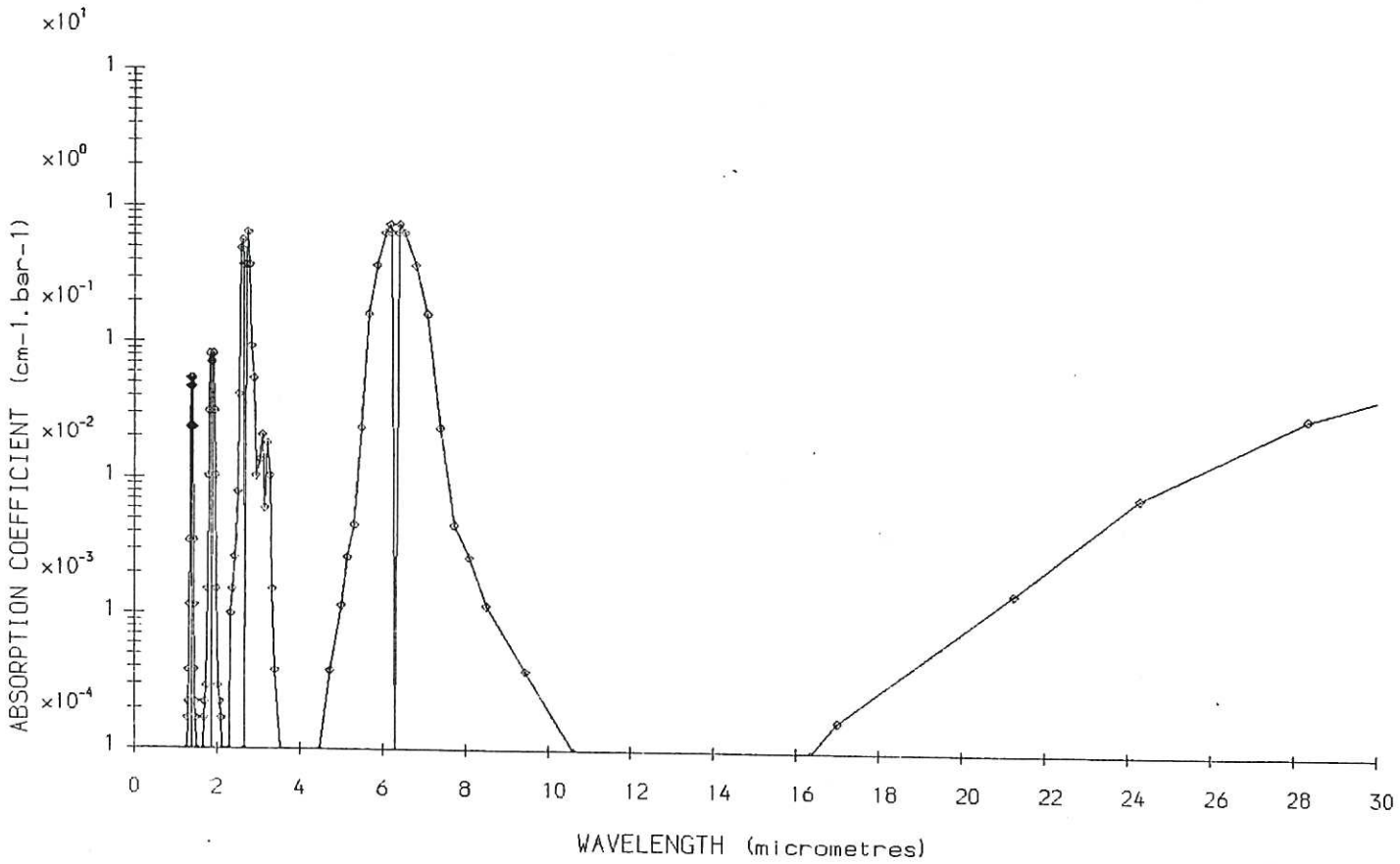

Fig. A5 The absorption coefficient of steam at 300K.

CLM-R252

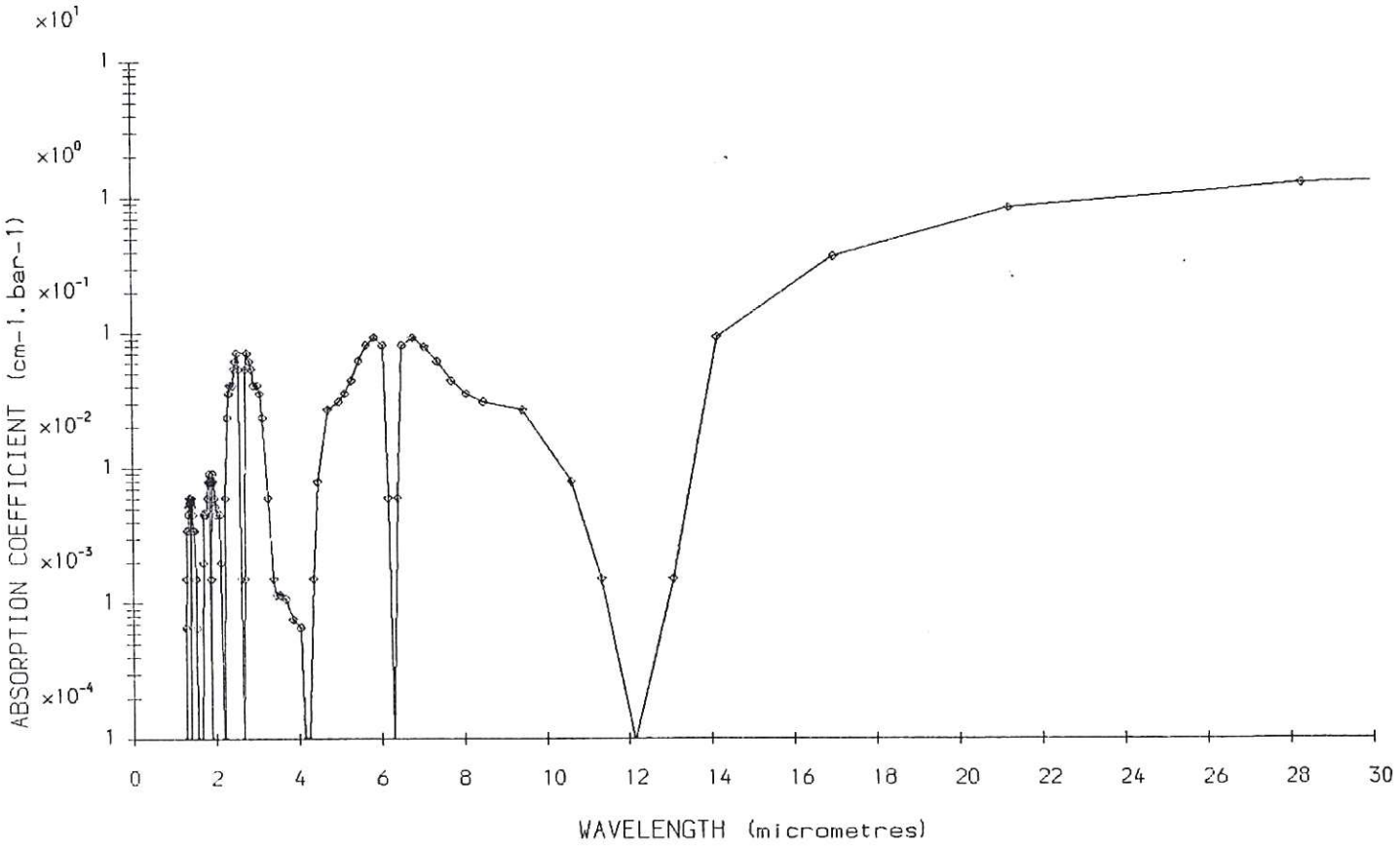

Fig. A6 The absorption coefficient of steam at 1000K.

CLM-R252

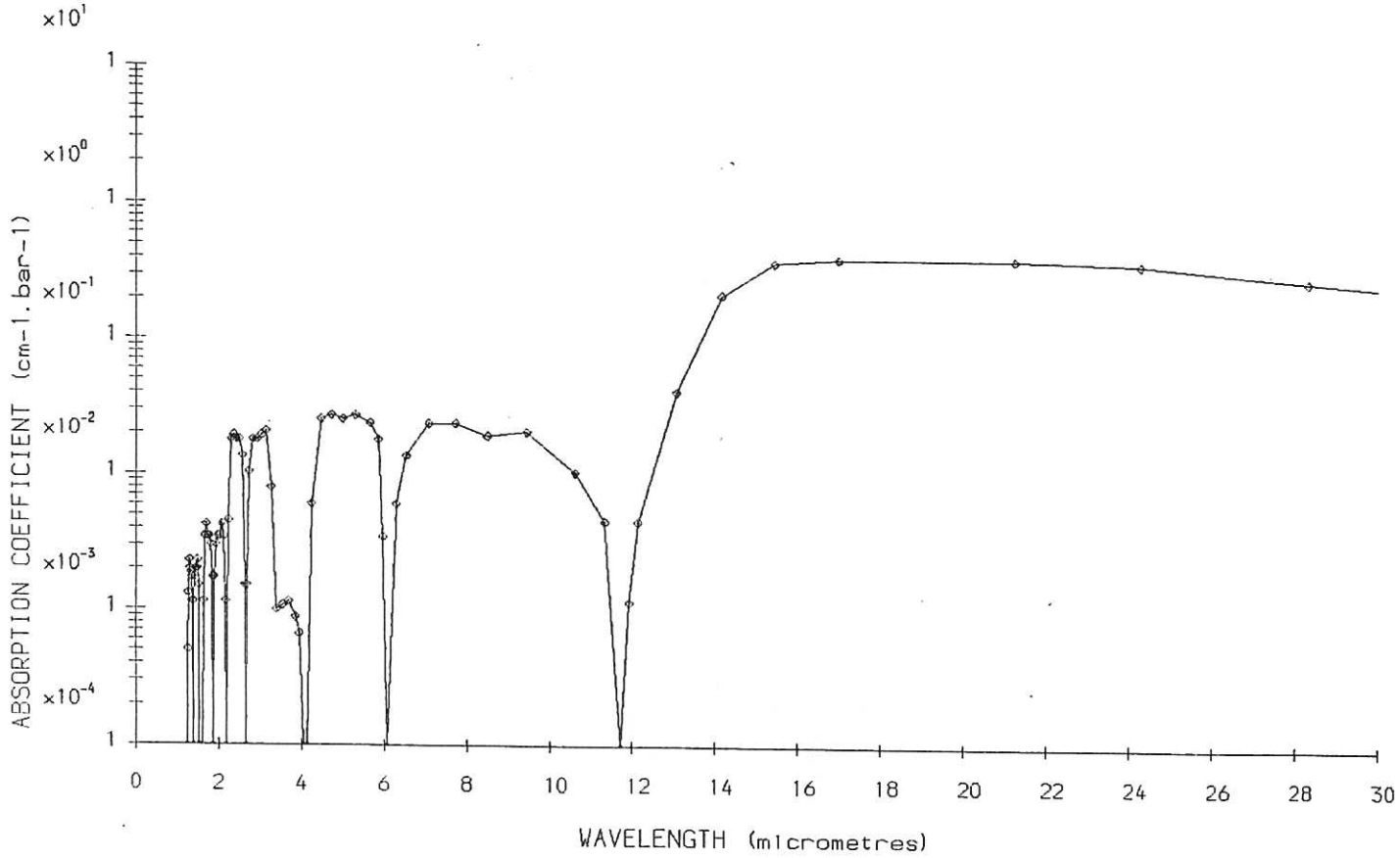

Fig. A7 The absorption coefficient of steam at 2000K.

CLM-R252

F. Hollman
EG 113

Available from
HER MAJESTY'S STATIONERY OFFICE
49 High Holborn, London, WC1V 6HB
(Personal callers only)
P.O. Box 276, London, SE1 9NH
(Trade orders by post)
13a Castle Street, Edinburgh, EH2 3AR
41 The Hayes, Cardiff, CF1 1JW
Princess Street, Manchester, M60 8AS
Southey House, Wine Street, Bristol, BS1 2BQ
258 Broad Street, Birmingham, B1 2HE
80 Chichester Street, Belfast, BT1 4JY

PRINTED IN ENGLAND